FUS regulates RAN translation through modulating the G-quadruplex structure of GGGGCC repeat RNA in *C9orf72*-linked ALS/FTD

Yuzo Fujino[1,2], Morio Ueyama[1,3,4], Taro Ishiguro[4,5], Daisaku Ozawa[1,3], Toshihiko Sugiki[6], Hayato Ito[7], Asako Murata[8], Akira Ishiguro[9], Tania F. Gendron[10], Kohji Mori[11], Eiichi Tokuda[12], Tomoya Taminato[1,3], Takuya Konno[13], Akihide Koyama[13], Yuya Kawabe[11], Toshihide Takeuchi[3,14], Yoshiaki Furukawa[12], Toshimichi Fujiwara[6], Manabu Ikeda[11], Toshiki Mizuno[2], Hideki Mochizuki[15], Hidehiro Mizusawa[5], Keiji Wada[4], Kinya Ishikawa[5], Osamu Onodera[13], Kazuhiko Nakatani[8], Hideki Taguchi[7,16], Leonard Petrucelli[10], and Yoshitaka Nagai[1,3,4,14,15]

[1] Department of Neurology, Kindai University Faculty of Medicine, Osaka-Sayama, Osaka 589-8511, Japan

[2] Department of Neurology, Kyoto Prefectural University of Medicine, Kyoto 602-0841, Japan

[3] Department of Neurotherapeutics, Osaka University Graduate School of Medicine, Suita, Osaka 565-0871, Japan

[4] Department of Degenerative Neurological Diseases, National Institute of Neuroscience, National Center of Neurology and Psychiatry, Kodaira, Tokyo 187-8502, Japan

[5] Department of Neurology and Neurological Science, Tokyo Medical and Dental University, Bunkyo-ku, Tokyo 113-8519, Japan

[6] Laboratory of Molecular Biophysics, Institute for Protein Research, Osaka University, Suita, Osaka 565-0871, Japan

[7] School of Life Science and Technology, Tokyo Institute of Technology, Yokohama, Kanagawa 226-8503, Japan

[8] Department of Regulatory Bioorganic Chemistry, The Institute of Scientific and Industrial Research, Osaka University, Ibaraki, Osaka 565-0047, Japan

[9] Research Center for Micro-nano Technology, Hosei University, Koganei, Tokyo 184-0003, Japan

[10] Department of Neuroscience, Mayo Clinic, Jacksonville, FL 32224, USA

[11] Department of Psychiatry, Osaka University Graduate School of Medicine, Suita, Osaka 565-0871, Japan

[12] Department of Chemistry, Keio University, Yokohama, Kanagawa 223-8522, Japan

[13] Department of Neurology, Clinical Neuroscience Branch, Brain Research Institute, Niigata University, Niigata 951-8585, Japan

[14] Life Science Research Institute, Kindai University, Osaka-Sayama, Osaka 589-8511, Japan

[15] Department of Neurology, Osaka University Graduate School of Medicine, Suita, Osaka 565-0871, Japan

[16] Cell Biology Center, Institute of Innovative Research, Tokyo Institute of Technology, Yokohama, Kanagawa 226-8503, Japan

*Correspondence

Department of Neurology
Kindai University Faculty of Medicine
377-2 Ohnohigashi, Osaka-Sayama, Osaka 589-8511, Japan
Tel.: +81 (72) 366-0246 (ext. 3553); Fax: +81 (72) 368-4846
E-mail: yoshi.nagai@med.kindai.ac.jp

Abstract

Abnormal expansions of GGGGCC repeat sequence in the noncoding region of the *C9orf72* gene is the most common cause of familial amyotrophic lateral sclerosis and frontotemporal dementia (C9-ALS/FTD). The expanded repeat sequence is translated into dipeptide repeat proteins (DPRs) by noncanonical repeat-associated non-AUG (RAN) translation. Since DPRs play central roles in the pathogenesis of C9-ALS/FTD, we here investigate the regulatory mechanisms of RAN translation, focusing on the effects of RNA-binding proteins (RBPs) targeting GGGGCC repeat RNAs. Using C9-ALS/FTD model flies, we demonstrated that the ALS/FTD-linked RBP FUS suppresses RAN translation and neurodegeneration in an RNA-binding activity-dependent manner. Moreover, we found that FUS directly binds to and modulates the G-quadruplex structure of GGGGCC repeat RNA as an RNA chaperone, resulting in the suppression of RAN translation *in vitro*. These results reveal a previously unrecognized regulatory mechanism of RAN translation by G-quadruplex-targeting RBPs, providing therapeutic insights for C9-ALS/FTD and other repeat expansion diseases.

Introduction

Amyotrophic lateral sclerosis (ALS) and frontotemporal dementia (FTD) are incurable neurodegenerative diseases with overlapping genetic and neuropathological features. Abnormal expansions of the GGGGCC (G_4C_2) repeat sequence in the noncoding region of the *C9orf72* gene have been found to be the most common genetic mutation responsible for ALS/FTD (DeJesus-Hernandez et al.; 2011, Gijselinck et al., 2012; Renton et al., 2011). Three major pathomechanisms are thought to be involved in the pathogenesis of *C9orf72*-linked ALS/FTD (C9-ALS/FTD): first, expansion of the G_4C_2 repeats results in decreased expression of the *C9orf72* gene, leading to its haploinsufficiency (Boivin et al., 2020; DeJesus-Hernandez et al. 2011; Gijselinck et al., 2012; Shi et al., 2018; Waite et al., 2014; Zhu et al., 2020). Second, the transcribed G_4C_2 repeat-containing RNA accumulates as RNA foci in the affected tissues, sequestering various RNA-binding proteins (RBPs) and altering their function (Conlon et al., 2016; Cooper-Knock et al., 2014; Donnelly et al., 2013; Haeusler et al., 2014; Lee et al., 2013; Mori et al., 2013a). Third, these G_4C_2 repeat RNA is also translated into dipeptide repeat (DPR) proteins, despite the lack of an AUG initiation codon, by noncanonical repeat-associated non-AUG (RAN) translation (Ash et al., 2013; Gendron et al., 2013; Mori et al., 2013b; Mori et al., 2013c; Zu et al, 2011; Zu et al, 2013). Since RAN translation occurs in all reading frames and the expanded G_4C_2 repeat sequence is bidirectionally transcribed, five distinct DPRs, i.e., poly(glycine-arginine) [poly(GR)], poly(glycine-alanine) [poly(GA)], poly(glycine-proline) [poly(GP)], poly(proline-arginine) [poly(PR)], and poly(proline-alanine) [poly(PA)] are produced and observed in patients' brains (Ash et al., 2013; Gendron et al., 2013; Mori et al., 2013b; Mori et al., 2013c; Zu et al., 2013) and cerebrospinal fluid (Gendron et al., 2017; Krishnon et

al., 2022; Lehmer et al., 2017; Su et al., 2014).

DPRs have been shown to exert toxic effects in multiple C9-ALS/FTD models, such as cultured cells, flies, and mice (Choi et al., 2019; Jovičić et al., 2015; May et al. 2014; Mizielinska et al., 2014; Rudich et al., 2017; Wen et al., 2014; Zhang et al., 2016; Zhang et al., 2018). Importantly, the toxicity of DPRs was confirmed in DPR-only flies, which express DPRs translated from non-G_4C_2 repeat RNAs with alternative codons and show neurodegeneration, whereas RNA-only flies expressing G_4C_2 repeat RNAs with stop codon interruptions, which eliminate DPRs production, did not show any obvious degenerative phenotypes (Mizielinska et al., 2014). In addition, increased DPR production, but not RNA foci, was reported to correlate with G_4C_2 repeat-induced toxicity in a C9-ALS/FTD *Drosophila* model (Tran et al., 2015). Taken together, these studies have strongly suggested that DPRs play a central role in the pathogenesis of C9-ALS/FTD. Indeed, DPRs have been reported to disrupt various biological pathways, such as nucleocytoplasmic transport (Hutten et al., 2020; Jovičić et al., 2015; Zhang et al., 2016) and membraneless organelle dynamics (Kwon et al., 2014; Lee et al., 2016; Lin et al., 2016). Therefore, elucidating the regulatory mechanism of RAN translation is a significant challenge toward developing potential therapies for C9-ALS/FTD.

Since the discovery of RAN translation in 2011 (Zu et al., 2011), many studies to date have focused on its molecular mechanisms, that is, whether it has functional overlap with canonical AUG-dependent translation. Previous studies on C9-ALS/FTD using monocistronic reporters containing a G_4C_2 repeat sequence revealed cap-dependent translation initiation from the upstream near-cognate CUG initiation codon, requiring the cap-binding eukaryotic translation factor 4F complex (Green et al., 2017; Tabet et al., 2018). On the other hand, studies using bicistronic reporters with a G_4C_2

114 repeat sequence in the second cistron also produced DPRs by RAN translation in all
115 reading frames, suggesting cap-independent translation initiation within the G_4C_2 repeat
116 sequence (Cheng et al., 2018; Sonobe et al., 2018). This is reminiscent of internal
117 ribosomal entry site translation initiation, which is another type of noncanonical cap-
118 independent translation in which specific factors are directly recruited to the highly-
119 structured mRNA for initiation (Kwan et al., 2019). While such initiation mechanisms
120 of RAN translation have been explored to date, specific roles of the repeat sequence on
121 RAN translation remain enigmatic. Considering a repeat length dependency of RAN
122 translation (Mori et al., 2013c; Zu et al., 2011; Zu et al., 2013), the repeat sequence
123 itself would also be essential for the initiation or elongation steps of RAN translation.
124 Based on our previous findings of the protective role of TDP-43 on UGGAA repeat-
125 induced toxicity in spinocerebellar ataxia type 31 (SCA31) models (Ishiguro et al.,
126 2017), we hypothesized that RBPs specifically binding to repeat sequences of template
127 RNA play a role in RAN translation.

128 Using *Drosophila* models of C9-ALS/FTD, we here demonstrate the regulatory
129 roles of the ALS/FTD-linked RBP FUS on RAN translation from G_4C_2 repeat RNA,
130 which lead to the significant modulation of neurodegeneration. We found that FUS
131 suppresses RNA foci formation and DPR production, resulting in the suppression of
132 repeat-induced degeneration. This suppressive effect on degeneration was abolished by
133 mutations in the RNA-recognition motif (RRM) of FUS. In contrast, knockdown of
134 endogenous *caz*, a *Drosophila* homologue of *FUS*, enhanced DPR aggregation and
135 RNA foci formation, resulting in the enhancement of repeat-induced degeneration.
136 Moreover, FUS was found to directly bind to G_4C_2 repeat RNA and modify its G-
137 quadruplex structure as an RNA chaperone, resulting in the suppression of RAN

138 translation *in vitro*. In addition, other G-quadruplex-targeting RBPs also suppressed
139 G_4C_2 repeat-induced toxicity in our C9-ALS/FTD flies. These results strongly indicate
140 that FUS regulates RAN translation and suppresses DPR toxicity through modulating
141 the G-quadruplex structure of G_4C_2 repeat RNA. Our findings shed light on the
142 regulatory mechanisms of RAN translation by G-quadruplex-targeting RBPs, and
143 propose novel therapeutic strategies for repeat expansion diseases by regulating RAN
144 translation.
145

146 ## Results

147 **Screening for RBPs that suppress G_4C_2 repeat-induced toxicity in C9-ALS/FTD**
148 **flies**

149 We established *Drosophila* models of C9-ALS/FTD that express pathogenic
150 length 42 or 89 G_4C_2 repeats [$(G_4C_2)_{42}$, or $(G_4C_2)_{89}$ flies, respectively], and confirmed
151 that expanded G_4C_2 repeat sequences induce eye degeneration and motor dysfunction
152 accompanied with the formation of RNA foci and the production of three types of DPRs
153 (Figure 1—figure supplement 1), consistent with previous studies (Freibaum et al.,
154 2015; Goodman et al., 2019; Mizielinska et al., 2014; Xu et al., 2013). We also
155 established *Drosophila* expressing normal length 9 G_4C_2 repeats as a control [$(G_4C_2)_9$
156 flies], and found that they did not show eye degeneration, motor dysfunction, RNA foci
157 formation, or DPR aggregation (Figure 1—figure supplement 1). We selected 18 RBPs
158 that have been reported to bind to G_4C_2 repeat RNA (Mori et al., 2013a), as well as
159 TDP-43, an ALS/FTD-linked RBP that does not bind to G_4C_2 repeat RNA (Xu et al.,
160 2013) (Figure 1—source data 1), and examined their roles in neurodegeneration in our
161 C9-ALS/FTD fly models. We found that coexpression of *FUS*, *IGF2BP1*, or

hnRNPA2B1 strongly suppressed the eye degeneration in both flies expressing $(G_4C_2)_{42 \text{ or } 89}$, which show decreased eye size and loss of pigmentation (Figures 1A–1D and Figure 1—source data 2). Coexpression of five RBPs, namely, *hnRNPR*, *SAFB2*, *SF3B3*, *hnRNPA1*, and *hnRNPL* also partially suppressed the eye degeneration, whereas coexpression of the other six RBPs had no effect, and two RBPs enhanced the phenotypes (Figures 1A–1D and Figure 1—source data 2). In addition, coexpression of *TDP-43* had no effect on the eye degeneration in $(G_4C_2)_{42}$ flies, and resulted in lethality in $(G_4C_2)_{89}$ flies, likely due to the toxicity of *TDP-43* expression itself (Figures 1A and 1D, and Figure 1—source data 2). The variation in the effects of these G_4C_2 repeat-binding RBPs on G_4C_2 repeat-induced toxicity may be due to their different binding affinities to G_4C_2 repeat RNA, and their different roles in RNA metabolism. We then analyzed the expression levels of G_4C_2 repeat RNA in flies coexpressing $(G_4C_2)_{89}$ and three RBPs that strongly suppressed eye degeneration. We found that coexpression of *IGF2BP1* or *hnRNPA2B1* significantly decreased G_4C_2 repeat RNA levels, whereas they were not altered upon coexpression of *FUS* (Figure 1E). Although the suppressive effects of IGF2BP1 and hnRNPA2B1 could simply be explained by the decreased levels of G_4C_2 repeat RNA, the molecular mechanisms by which FUS suppresses G_4C_2 repeat-induced toxicity remain to be clarified. The suppressive effects of FUS on G_4C_2 repeat-induced toxicity was confirmed using multiple FUS fly lines, showing the significant suppression of decreased eye size and loss of pigmentation in $(G_4C_2)_{42 \text{ or } 89}$ flies coexpressing *FUS* (Figure 1—figure supplement 2). Therefore, we decided to further focus on FUS, which is another ALS/FTD-linked RBP, and investigated its mechanism of the suppression of G_4C_2 repeat-induced toxicity.

FUS suppresses G_4C_2 repeat-induced toxicity via its RNA-binding activity

We next investigated whether the suppressive effects of FUS on G_4C_2 repeat-induced toxicity are mediated by its binding to G_4C_2 repeat RNA, using flies expressing FUS with mutations in the RRM (*FUS-RRMmut*), which have been reported to eliminate its RNA-binding activity (Daigle et al., 2013). Western blot analysis confirmed that the *FUS-RRMmut* fly line expresses almost an equivalent level of the FUS proteins to the *FUS* fly line (Figure 2—figure supplement 1). We found that coexpression of *FUS-RRMmut* did not restore the eye degeneration in flies expressing $(G_4C_2)_{89}$, suggesting that the RNA-binding activity of FUS is essential for its suppressive effects on G_4C_2 repeat-induced toxicity (Figures 2A–C). We also evaluated the reduced egg-to-adult viability of $(G_4C_2)_{42}$ flies, and confirmed that this phenotype was rescued by coexpression of *FUS*, but not by coexpression of *FUS-RRMmut* (Figure 2D). Expression of G_4C_2 repeat RNA in the nervous system of flies after eclosion using the *elav-GeneSwitch* driver induces motor dysfunction, and coexpression of *FUS* significantly alleviated this motor dysfunction (Figure 2E), indicating that FUS suppresses the neuronal phenotypes of flies expressing G_4C_2 repeat RNA. It is notable that the motor dysfunction caused by the expression of *FUS* alone was also alleviated by coexpression of $(G_4C_2)_{42}$ (Figure 2E), indicating that the G_4C_2 repeat RNA conversely suppresses FUS toxicity. This result is consistent with our previous observations in SCA31 flies that UGGAA repeat RNA reduced the aggregation and toxicity of TDP-43 (Ishiguro et al., 2017). Moreover, recent studies demonstrated that RNA buffers the phase separation of TDP-43 and FUS, resulting in the suppression of their aggregation (Maharana et al., 2018; Mann et al., 2019). These findings hence suggest that balancing the crosstalk between repeat RNAs and RBPs neutralizes the

toxicities of each other.

FUS suppresses RNA foci formation and RAN translation from G_4C_2 repeat RNA

We next analyzed the effects of FUS expression on RNA foci and DPR production in flies expressing G_4C_2 repeat RNA. We performed RNA fluorescence *in situ* hybridization (FISH) of the salivary glands of fly larvae expressing $(G_4C_2)_{89}$, and found that coexpression of *FUS* significantly decreased the number of nuclei containing RNA foci in $(G_4C_2)_{89}$ flies, whereas it was not altered by coexpression of *FUS-RRMmut* (Figures 3A and 3B). We confirmed that the expression levels of G_4C_2 repeat RNA in $(G_4C_2)_{89}$ flies were not altered by coexpression of *FUS* or *FUS-RRMmut* (Figure 3C). These results were in good agreement with our previous study on SCA31 showing the suppressive effects of FUS and other RBPs on RNA foci formation of UGGAA repeat RNA as RNA chaperones (Ishiguro et al., 2017), raising the possibility that FUS has RNA-chaperoning activity also for G_4C_2 repeat RNA. Immunohistochemistry of the eye imaginal discs of fly larvae expressing $(G_4C_2)_{89}$ revealed that coexpression of *FUS* significantly decreased the number of DPR aggregates in $(G_4C_2)_{89}$ flies, whereas coexpression of *FUS-RRMmut* did not (Figures 3D and 3E). Quantitative analyses of poly(GP) by immunoassay also demonstrated that poly(GP) levels were greatly decreased in $(G_4C_2)_{89}$ flies upon coexpression of *FUS*, but not *FUS-RRMmut* (Fig 3F), indicating that FUS suppresses RAN translation from the G_4C_2 repeat RNA to reduce DPR production. Considering that the 5′ upstream sequence of the G_4C_2 repeat in the *C9orf72* gene is reported to affect RAN translation activity (Green et al., 2017; Tabet et al., 2018), we used flies expressing the G_4C_2 repeat sequence with the upstream intronic sequence of the *C9orf72* gene, namely, *LDS*-$(G_4C_2)_{44}^{\text{GR-GFP}}$ (Goodman et al., 2019).

234 Since this construct has a 3′-green fluorescent protein (GFP) tag in the GR reading
235 frame downstream of the G_4C_2 repeat sequence, the GR-GFP fusion protein is produced
236 by RAN translation. We confirmed that coexpression of *FUS* significantly decreased the
237 expression level of GR-GFP, whereas coexpression of *FUS-RRMmut* had no effect
238 (Figures 3G–3I).

239 We further excluded the possibility that FUS directly interacts with DPRs, rather
240 than with G_4C_2 repeat RNA, to decrease DPR levels and exert its suppressive effects.
241 Using DPR-only flies expressing DPRs translated from non-G_4C_2 RNAs with
242 alternative codons (Mizielinska et al., 2014), we confirmed that FUS did not suppress
243 the eye degeneration in DPR-only flies expressing poly(GR), but rather enhanced their
244 phenotypes, likely due to the additive effects of FUS toxicity (Figure 3—figure
245 supplement 1). Together with the finding that FUS decreases not only DPR expression
246 but also RNA foci formation (Figures 3A and 3B), these results collectively indicate that
247 FUS indeed interacts with G_4C_2 repeat RNA and regulates RAN translation from G_4C_2
248 repeat RNA in *Drosophila* models of C9-ALS/FTD.

249

250 **Reduction of endogenous *caz* expression enhances G_4C_2 repeat-induced toxicity,**
251 **RNA foci formation, and DPR aggregation**

252 To elucidate the physiological role of FUS on RAN translation, we also
253 investigated the role of endogenous *caz*, a *Drosophila* homologue of *FUS*, on G_4C_2
254 repeat-induced toxicity in flies expressing G_4C_2 repeat RNAs. Coexpression of *caz* as
255 well as *FUS* suppressed eye degeneration in flies expressing $(G_4C_2)_{42 \text{ or } 89}$ (Figure 4—
256 figure supplement 1). These data suggest that *caz* is a functional homologue of *FUS*. In
257 contrast, knockdown of *caz* by RNA interference or its hemizygous deletion modestly

258 but significantly enhanced the eye degeneration in $(G_4C_2)_{89}$ flies (Figures 4A–4D),
259 indicating that reduced *caz* expression enhances G_4C_2 repeat-induced toxicity. We next
260 analyzed the effects of *caz* knockdown on RNA foci formation and DPR production in
261 flies expressing $(G_4C_2)_{89}$. FISH analysis of the salivary glands revealed that knockdown
262 of *caz* significantly increased the number of nuclei containing RNA foci in $(G_4C_2)_{89}$
263 flies (Figures 4E and 4F). We also confirmed that the expression levels of G_4C_2 repeat
264 RNA in $(G_4C_2)_{89}$ flies were not altered by the knockdown of *caz* (Figure 4G).
265 Immunohistochemical analysis showed that knockdown of *caz* significantly increased
266 the number of DPR aggregates in $(G_4C_2)_{89}$ flies (Figures 4H and 4I). These results
267 indicate that the reduction of *caz* expression enhances RNA foci formation and DPR
268 aggregation, compatible with the results of *FUS* coexpression in flies expressing
269 $(G_4C_2)_{89}$ (Figure 3), and that FUS functions as an endogenous regulator of RAN
270 translation.
271
272 **FUS directly binds to and modulates the G-quadruplex structure of G_4C_2 repeat**
273 **RNA, resulting in the suppression of RAN translation *in vitro***
274 We next confirmed the direct interaction of FUS with G_4C_2 repeat RNA by the
275 filter binding assay. We found that His-tagged FUS binds to the $(G_4C_2)_4$ RNA in a dose-
276 dependent manner, but not to the control $(AAAAAA)_4$ RNA (Figure 5A), and His-
277 tagged FUS-RRMmut had almost no binding affinity to the $(G_4C_2)_4$ RNA, consistent
278 with a previous study (Mori et al., 2013a). We also confirmed the interaction of FUS
279 with the G_4C_2 repeat RNA in our C9-ALS/FTD flies by showing the colocalization of
280 FUS with the RNA foci (Figure 5—figure supplement 1), consistent with a recent study
281 using C9-ALS/FTD patient fibroblasts (Bajc Česnik et al., 2019). Since G_4C_2 repeat

282 RNA was reported to form both G-quadruplex and hairpin structures (Fratta et al., 2012;
283 Hauesler et al., 2014; Reddy et al., 2013; Su et al., 2014), we next characterized the
284 interactions of FUS with G_4C_2 repeat RNA having different structures. G_4C_2 repeat
285 RNA is known to form G-quadruplex structures in the presence of K^+, whereas they
286 form hairpin structures in the presence of Na^+ (Su et al., 2014). Surface plasmon
287 resonance (SPR) analyses demonstrated that FUS preferentially binds to $(G_4C_2)_4$ RNA
288 with the G-quadruplex structure in KCl buffer (Table 1, dissociation constant (K_D) =
289 1.5×10^{-8} M), and weakly to $(G_4C_2)_4$ RNA with the hairpin structure in NaCl buffer
290 (Table 1, $K_D = 1.3\times10^{-7}$ μM). We also confirmed that FUS has poor binding affinity to
291 $(G_4C_2)_4$ RNA in LiCl buffer (Table 1, $K_D = 1.4\times10^{-5}$ μM), which destabilizes the G-
292 quadruplex structure (Herdy et al., 1992), and was an almost similar level to its binding
293 affinity to the negative control $(A_4C_2)_4$ RNA (not shown). These results suggest the
294 preferential binding of FUS to G_4C_2 repeat RNA with the G-quadruplex structure,
295 which is consistent with a previous report showing preferential binding of FUS to G-
296 quadruplex structured Sc1 and DNMT RNAs (Ozdilek et al., 2017). Considering that
297 higher-order structures, including G-quadruplex and hairpin structures, are reported to
298 be involved in RAN translation (Mori et al., 2021; Simone et al., 2018; Wang et al.,
299 2019; Zu et al., 2011), we next investigated the effects of FUS on the structure of G_4C_2
300 repeat RNA. The circular dichroism (CD) spectrum of $(G_4C_2)_4$ RNA in KCl buffer was
301 found to exhibit a positive peak at approximately 260 nm and a negative peak at 240 nm
302 (Figure 5B, black line), consistent with previous reports (Fratta et al., 2012; Hauesler et
303 al., 2014; Reddy et al., 2013; Su et al., 2014). Interestingly, upon the addition of FUS,
304 these two peaks were notably shifted to longer wavelengths with substantial CD
305 spectrum changes, indicating a significant structural alteration in $(G_4C_2)_4$ RNA (Figure

306 5B, red line). We confirmed that the CD spectrum of FUS alone in the wavelength range
307 of 240 to 300 nm was almost negligible (Figure 5—figure supplement 2A, green line),
308 indicating that this change in CD spectrum is attributed to structural changes in the
309 $(G_4C_2)_4$ RNA. We also observed CD spectrum changes to some extent in the $(G_4C_2)_4$
310 RNA upon the addition of FUS in NaCl buffer, but not in LiCl buffer, confirming an
311 interaction between FUS and hairpin-structured $(G_4C_2)_4$ RNA as well (Figures 5C and
312 5D). We further analyzed the interaction between FUS and G_4C_2 repeat RNA by imino
313 proton nuclear magnetic resonance (NMR). In KCl buffer, the NMR signals of the
314 imino proton for the G-quadruplex structure of $(G_4C_2)_4$ RNA were detected in the region
315 around 10 to 12 ppm (Figure 5—figure supplement 2D), consistent with previous
316 studies (Fratta et al., 2012; Su et al., 2014). Upon the addition of FUS, the NMR
317 intensities of $(G_4C_2)_4$ RNA were decreased in an FUS concentration-dependent manner
318 (Figure 5—figure supplement 2D), further supporting the possibility that that FUS
319 interacts with and modulates the G-quadruplex structure of $(G_4C_2)_4$ RNA. Collectively,
320 these results indicate that FUS directly binds to G_4C_2 repeat RNA, preferentially to its
321 G-quadruplex form, and modulates its higher-order structures. These structural
322 alterations of G_4C_2 repeat RNAs by FUS did not require ATP or interactions with other
323 proteins, suggesting its role as an RNA chaperone for G_4C_2 repeat RNA (Rajkowitsch et
324 al., 2007).

325 To further clarify the direct link between the binding of FUS to G_4C_2 repeat
326 RNA and its effects on RAN translation, we employed a cell-free *in vitro* translation
327 assay using rabbit reticulocyte lysate. We designed a reporter construct containing the
328 80 G_4C_2 repeat sequence with the 5′ upstream intronic sequence of the *C9orf72* gene
329 and the Myc tag sequence in the GA reading frame at the 3′ downstream (Figure 5E).

This upstream sequence contained multiple stop codons in each reading frame and lacked AUG initiation codons. We confirmed by Western blotting that this reporter system indeed produces GA-Myc by RAN translation, consistent with previous studies (Green et al., 2017; Tabet et al., 2018). Notably, the addition of FUS to this system decreased the expression level of GA-Myc in a dose-dependent manner, whereas the addition of the control bovine serum albumin (BSA) did not (Figure 5F). Taken together, these results indicate that FUS suppresses RAN translation from G_4C_2 repeat RNA *in vitro* as an RNA chaperone.

Identification of G-quadruplex-targeting RBPs that suppress G_4C_2 repeat-induced toxicity in C9-ALS/FTD flies

Considering that FUS suppresses G_4C_2 repeat-induced toxicity as an RNA chaperone through its preferential binding to the G-quadruplex structure of G_4C_2 repeat RNA (Figure 5 and Table 1), we hypothesized that other G-quadruplex-targeting RBPs might have similar suppressive effects on G_4C_2 repeat-induced toxicity. To investigate this possibility, we selected 6 representative G-quadruplex-targeting RBPs, all of which are known to bind to G_4C_2 RNA as well (Cooper-Knock et al., 2014; Haeusler et al., 2014; Mori et al., 2013a; Xu et al., 2013) (Figure 6—source data 1). Intriguingly, coexpression of *EWSR1*, *DDX3X*, *DDX5*, or *DDX17* significantly suppressed eye degeneration in $(G_4C_2)_{89}$ flies without altering G_4C_2 RNA expression (Figure 6). Their effects on G_4C_2 repeat-induced toxicity and repeat RNA expression were consistent with those of FUS. In support of our results, DDX3X was previously reported to suppress RAN translation and G_4C_2 repeat-induced toxicity in cell culture in a helicase-activity-dependent manner (Cheng et al., 2019). On the other hand, coexpression of *DHX9* or

354 *DHX36* suppressed eye degeneration by reducing G_4C_2 repeat RNA levels (Figure 6).
355 Since G-quadruplex-targeting RBPs have diverse biological functions, including
356 transcription, RNA processing, translation, and RNA stabilization (Dumas et al., 2021),
357 these different effects among G-quadruplex-targeting RBPs on G_4C_2 repeat RNA
358 expression might be attributed to their different roles in RNA metabolism. Thus, some
359 G-quadruplex-targeting RBPs regulate G_4C_2 repeat-induced toxicity by binding to and
360 possibly by modulating the G-quadruplex structure of G_4C_2 repeat RNA.
361

Discussion

In this study, we revealed a novel regulatory mechanism of RAN translation from expanded G_4C_2 repeat RNA by the ALS/FTD-linked RBP FUS, which suppresses DPR production and neurodegeneration in C9-ALS/FTD *Drosophila* models (Figures 1–4). FUS directly binds to G_4C_2 repeat RNA and modulates its G-quadruplex structure, as evident by CD and NMR analyses (Figure 5), suggesting its functional role as an RNA chaperone. This is reminiscent of our recent study on SCA31, in which we demonstrated a novel role of the ALS/FTD-linked RBPs TDP-43, FUS, and hnRNPA2B1 as RNA chaperones binding to UGGAA repeat RNA and altering its structure, resulting in the suppression of its neurotoxicity through reducing RNA foci formation and repeat polypeptide translation (Ishiguro et al., 2017). Considering the similarities of the effects of FUS on G_4C_2 repeat RNA and UGGAA repeat RNA, we conclude that FUS functions as an RNA chaperone also for G_4C_2 repeat RNA to regulate its RAN translation.

The suppressive effects of RBPs in several noncoding repeat expansion diseases by the amelioration of their sequestration into RNA foci have been reported. For example, in myotonic dystrophy type 1, MBNL1 was shown to be sequestered into CUG repeat RNA foci, and overexpression of MBNL1 in a mouse model was found to compensate its functional loss, resulting in the reversal of myotonia (Kanadia et al., 2006). Similarly, previous studies reported the suppressive effects of other RBPs on neurodegeneration, such as hnRNPA2B1 in fragile X ataxia/tremor syndrome (Sofora et al., 2007), and Pur-α and Zfp106 in C9-ALS/FTD (Xu et al., 2013; Celona et al., 2017). The suppressive effects of these RBPs have been thought to result from the supplementation against their loss-of-function due to their sequestration into RNA foci,

386 although their effects on gain-of-toxic disease pathomechanisms, that is, RAN
387 translation and repeat RNA expression, remain to be elucidated. In contrast, in this
388 study we demonstrated that FUS suppresses neurodegeneration in C9-ALS/FTD by
389 directly targeting G_4C_2 repeat RNA and inhibiting RAN translation as an RNA
390 chaperone. Similar suppressive effects of RBPs by targeting UGGAA repeat RNA in
391 SCA31 as RNA chaperones have also been reported (Ishiguro et al., 2017). In addition,
392 we also showed that the expression of IGF2BP1, hnRNPA2B1, DHX9, and DHX36
393 decreased G_4C_2 repeat RNA expression and suppressed eye degeneration in our C9-
394 ALS/FTD *Drosophila* model (Figures 1 and 6), likely via the reduction of DPR levels.
395 In myotonic dystrophy type 2 models, MBNL1 was also reported to retain CCUG repeat
396 RNA in the nucleus, resulting in the suppression of RAN translation (Zu et al., 2017),
397 implying various mechanisms of the effects of RBPs depending on the combination of
398 RBPs and repeat RNA. Nevertheless, our findings highlighted the previously
399 unrecognized roles of RBPs directly interacting with repeat RNA and modulating gain-
400 of-toxic pathomechanisms, including RAN translation in noncoding repeat expansion
401 diseases.

402 Several studies have indicated the importance of higher-order structures of repeat
403 RNA in RAN translation. In SCA8 models, hairpin-forming CAG repeat RNA was
404 shown to be RAN-translated to produce polyglutamine proteins, but switching the CAG
405 repeats to non-hairpin-forming CAA repeats abolished the RAN translation (Zu et al.,
406 2011). In C9-ALS/FTD, G_4C_2 repeat RNA has been reported to form both hairpin and
407 G-quadruplex structures (Fratta et al., 2012; Hauesler et al., 2014; Reddy et al., 2013;
408 Su et al., 2014). Although the effect of each structure on RAN translation remains
409 largely unknown, small molecules binding to the hairpin structure or the G-quadruplex

410 structure were both reported to inhibit RAN translation from the G_4C_2 repeat RNA,
411 resulting in reduced DPR levels (Wang et al., 2019, Mori et al., 2021). These findings
412 are in accordance with our results showing that FUS modifies the G-quadruplex
413 structure as well as the hairpin structure of G_4C_2 repeat RNA as an RNA chaperone and
414 reduces DPR production. We further found that G-quadruplex-targeting RNA helicases,
415 including DDX3X, DDX5, and DDX17, which are known to bind to G_4C_2 repeat RNA
416 (Cooper-Knock et al., 2014; Haeusler et al., 2014; Mori et al., 2013a; Xu et al., 2013),
417 also alleviate G_4C_2 repeat-induced toxicity without altering the expression levels of
418 G_4C_2 repeat RNA in our *Drosophila* models. These results suggest that not only ATP-
419 independent RNA chaperones, but also ATP-dependent RNA helicases may regulate
420 RAN translation through modifying the higher-order structures of template repeat RNA.
421 Consistently, a previous study also reported that DDX3X inhibits RAN translation from
422 G_4C_2 repeat RNA in a helicase activity-dependent manner (Cheng et al., 2019).
423 Knockdown of another RNA helicase, DHX36, has been reported to both promote
424 (Cheng et al., 2019) and inhibit (Liu et al., 2021; Tseng et al., 2021) RAN translation,
425 possibly due to the different effects on repeat RNA structures depending on the
426 experimental conditions. Unfortunately, most of these studies reporting the effects of
427 RBPs on RAN translation have limitations of the detailed structural analyses of repeat
428 RNA. In this study, focusing on FUS, we performed a series of molecular structural
429 analyses, *in vitro* translation assays, and *in vivo* genetic analyses to clarify the structure-
430 function relationship of G_4C_2 repeat RNA, and provide compelling evidence for the
431 modifying effects of FUS on repeat RNA structures leading to the suppression of RAN
432 translation and repeat-induced toxicity *in vivo*.

433 FUS has an RRM domain for RNA binding and a low complexity (LC) domain

434 involved in protein interactions, and exerts multifaceted functions, such as RNA
435 transcription, RNA splicing, RNA transport, and formation of membraneless organelles,
436 such as stress granules and nuclear paraspeckles via liquid-liquid phase separation
437 (Lagier-Tourenne et al., 2010). Recent studies reported that arginine-rich DPRs, such as
438 poly(GR) and poly(PR), interact with LC domain-containing RBPs, including FUS, and
439 alter their liquid-liquid phase separation, resulting in the disruption of the dynamics and
440 functions of membraneless organelles (Kwon et al., 2014; Lee et al., 2016; Lin et al.,
441 2016). These findings raise the possibility that FUS may exert its suppressive effects by
442 directly interacting with DPRs. However, we showed that FUS does not suppress eye
443 degeneration in DPR-only flies (Figure 3—figure supplement 1) indicating that a direct
444 interaction between FUS and DPRs is unlikely to be the mechanism of the suppression
445 of DPR toxicity in our C9-ALS/FTD flies. This result supports our conclusion that FUS
446 suppresses G_4C_2 repeat-induced toxicity through direct binding to G_4C_2 repeat RNA.
447 In summary, we here provided evidence that FUS modulates the structure of G_4C_2
448 repeat RNA as an RNA chaperone, and regulates RAN translation, resulting in the
449 suppression of neurodegeneration in C9-ALS/FTD fly models. Recent advances in
450 genome sequencing technology unveiled that such expansions of repeat sequences cause
451 more than 50 monogenic human diseases (Malik et al., 2021), and are also associated
452 with psychiatric diseases such as autism (Mitra et al., 2021; Trost et al., 2020). Thus,
453 our findings contribute not only towards the elucidation of repeat-associated pathogenic
454 mechanisms underlying a wider range of neuropsychiatric diseases than previously
455 thought, but also towards the development of potential therapies for these diseases.
456

Materials and Methods

Flies

All fly stocks were cultured and crossed at 23 °C or 25 °C in standard cornmeal-yeast-glucose medium. Male adult flies were used for the climbing assay and *GeneSwitch* experiments. Three to 5-day-old female adult flies were used for the evaluation of eye phenotype using a stereoscopic microscope model SZX10 (Olympus). Female third instar larvae were used for quantitative real-time polymerase chain reaction (PCR), RNA FISH and immunohistochemistry experiments. The transgenic fly line bearing the *GMR-Gal4* transgene has been described previously (Yamaguchi et al., 1999). The transgenic fly lines bearing *elav-Gal4* (#8765), *elav-GeneSwitch* (#43642), *UAS-EGFP* (#6874), *UAS-DsRed* (#6282), *UAS-GFP-IR* (inverted repeat) (#9330), *UAS-*$(GR)_{36}$ (#58692), *UAS-*$(GA)_{36}$ (#58693), *UAS-*$(GR)_{100}$ (#58696), *UAS-*$(GA)_{100}$ (#58697), and *UAS-EWSR1* (#79592) were obtained from Bloomington Drosophila Stock Center. The transgenic fly line bearing *UAS-caz-IR* (#100291) was obtained from Vienna Drosophila Resource Center. The fly line with the *caz* null allele (caz^2), *UAS-LDS-*$(G_4C_2)_{44}^{\text{GR-GFP}}$, and *UAS-caz* (*UAS-FLAG-caz*) and *UAS-FUS*-4 (*UAS-FLAG-FUS*) were kind gifts from Dr. Erik Storkebaum (Frickenhaus et al., 2015), Dr. Nancy Bonini (Goodman et al., 2019), and Dr. Brian McCabe (Wang et al., 2011), respectively. Other transgenic fly lines were generated in this study. Full genotypes of the fly lines used in all figures and their cultured temperatures are described in Supplementary file 1.

Generation of constructs and transgenic flies

Artificially synthesized $(G_4C_2)_{50}$ sequences flanked at the 5′ end with an *Eag*I recognition site and at the 3′ end with a *PspOM*I recognition site were subcloned into T-

481 vector pMD20 (Takara Bio). To generate a longer repeat size, the pMD20-(G_4C_2)$_{50}$
482 vector was digested with *Eag*I and *PspOM*I, followed by ligation into the pMD20-
483 (G_4C_2)$_{50}$ vector linearized by digestion with *Eag*I. This vector was digested with *EcoR*I
484 and *Hind*III, and subcloned into the pcDNA™3.1/*myc*-His(−)A vector (Thermo Fisher
485 Scientific). We accidentally obtained the pcDNA™3.1/*myc*-His(−)A-(G_4C_2)$_9$ vector at
486 this step. The pcDNA™3.1/*myc*-His(−)A-(G_4C_2)$_n$ vector was digested with *EcoR*I and
487 *Xba*I, and subcloned into the *Drosophila* pUAST vector. These constructs have no start
488 codon sequence (ATG) upstream of the G_4C_2 repeat sequence (Figure 1—figure
489 supplement 1A). These pUAST-(G_4C_2)$_n$ vectors were amplified with a recombinase-
490 mutated SURE®2 *Escherichia coli* strain (Agilent Technologies) at 28 °C for 72 hours
491 to prevent repeat length contraction. The number of G_4C_2 repeats in the pUAST-(G_4C_2)$_9$
492 $_{or\ 50}$ vectors was determined by sequencing. To determine the number of G_4C_2 repeats in
493 the pUAST-(G_4C_2)$_{89}$ vector, transposable element insertional mutagenesis using EZ-
494 Tn5™ <KAN-2> Insertion Kit (Epicentre) and sequencing were performed.

495 To generate pUAST-*FUS* or pUAST-*TDP-43* vectors, the Gateway® Vector
496 Conversion System (Thermo Fisher Scientific) was used. The human *FUS* or human
497 *TARDBP* cDNA was subcloned into the pENTR™/D-TOPO® vector (Thermo Fisher
498 Scientific). To generate the Gateway destination vector pUAST-DEST, we inserted the
499 Gateway cassette A sequence (Thermo Fisher Scientific) into the pUAST vector. The
500 pUAST-*FUS* or pUAST-*TDP-43* vectors were generated using Gateway recombination
501 reactions (Thermo Fisher Scientific) . The FUS RRM mutant construct (pUAST-*FUS*-
502 *RRMmut*), in which leucine residues at positions 305, 341, 359, and 368 in the FUS
503 protein were substituted to phenylalanine, was generated by PCR and the In-Fusion®
504 Cloning system (Takara Bio). To generate the other pUASTattB-*RBP* vectors, each

505 cDNA encoding the RBP shown in Figure 1—source data 1 and Figure 6—source data 1
506 was subcloned into the pUASTattB vector (VectorBuilder). To establish transgenic flies
507 harboring *UAS*-$(G_4C_2)_n$, *UAS-FUS*, *UAS-FUS-RRMmut*, and *UAS-TDP-43*, the pUAST-
508 $(G_4C_2)_n$, pUAST-*FUS*, pUAST-*FUS* line 2, pUAST-*FUS-RRMmut*, and pUAST-*TDP-*
509 *43* vectors, respectively, were injected into fly embryos of the w^{1118} strain. To establish
510 transgenic flies harboring the other *UAS-RBP* constructs including *UAS-FUS* line 3,
511 pUASTattB-*RBP* vectors were injected into fly embryos of the attP40 strain. These
512 transgenic flies were established using standard methods at BestGene Inc.

513 The number of repeats in *UAS*-$(G_4C_2)_{9\ \mathrm{or}\ 42}$ transgenic flies were determined by
514 genomic PCR using the forward (5′-AACCAGCAACCAAGTAAATCAAC-3′), and
515 reverse (5′-TGTTGAGAGTCAGCAGTAGCC-3′) primers, which amplifies a part of
516 the *UAS*-$(G_4C_2)_n$ sequence, including G_4C_2 repeat sequence, followed by sequencing
517 using the forward (5′-GCCAAGAAGTAATTATTGA-3′) and/or reverse (5′-
518 TCCAATTATGTCACACC-3′) primers.

519

520 **Quantitative real-time PCR**

521 Total RNA was extracted from female third instar larvae of each genotype using
522 TRIzol® reagent (Thermo Fisher Scientific) according to the manufacturer's
523 instructions. First-strand cDNA was synthesized using QuantiTect Reverse
524 Transcription Kit (QIAGEN). Real-time PCR was performed using SYBR® Premix Ex
525 Taq™ II (Takara Bio) and the Mx3000P Real-time quantitative PCR system (Agilent
526 Technologies) or the CFX96™ Real-Time PCR Detection System (Bio-Rad). For G_4C_2
527 repeat RNA quantification of flies expressing $(G_4C_2)_n$ in Figure 1—figure supplement
528 1C, the forward (5′-ATGAATGGGAGCAGTGGTGG-3′) and reverse (5′-

529 TGTTGAGAGTCAGCAGTAGCC-3′) primers were used. For G_4C_2 repeat RNA
530 quantification of flies expressing $(G_4C_2)_{89}$(H) and FUS, FUS-RRMmut, other RNA-
531 binding proteins, or *caz-IR* in Figures 1E, 3C, 4G, and 6D, the forward (5′-
532 CCCAATCCATATGACTAGTAGATCC-3′) and reverse (5′-
533 TGTAGGTAGTTTGTCCAATTATGTCA-3′) primers were used. Both of the above-
534 mentioned primer pairs recognize sequences downstream of the G_4C_2 repeats. For *gal4*
535 mRNA quantification, the forward (5′-TTGAAATCGCGTCGAAGGA-3′) and reverse
536 (5′-GGCTCCAATGGCTAATATGCA-3′) primers were used (Li et al., 2008). Data were
537 analyzed using the standard curve method. The amounts of G_4C_2 repeat transcripts were
538 normalized to those of *gal4* transcripts in the same sample. At least three independent
539 biological replicates per genotype were analyzed. Data were normalized by setting the
540 values of the samples from flies expressing $(G_4C_2)_{89}$(H) (Figure 1—figure supplement
541 1C), both $(G_4C_2)_{89}$(H) and *EGFP* (Figures 1E, 3C, and 6D), or both $(G_4C_2)_{89}$(H) and
542 *GFP-IR* (Figure 4G) as 100.
543
544 **Imaging and quantification of fly eyes**
545 Light microscopic images of the eyes of 3 to 5-day-old female flies were taken
546 using a stereoscopic microscope model SZX10 (Olympus) with a CCD camera DP21
547 (Olympus). Images shown are representative eye phenotypes of the fly crosses. Crosses
548 were performed three times to validate the specific phenotypes. Eye size and
549 pigmentation were quantified as previously reported (Saitoh et al., 2015). Five or 10
550 eyes per genotype were analyzed. Data were normalized by setting the values of
551 samples from flies expressing one copy of *EGFP* (Figure 4D), those expressing two

552 copies of *EGFP* (Figures 1B, 1C, 1D, 2B, 2C, 6B, 6C, Figure 1—figure supplements
553 2B-2D, and Figure 4—figure supplements 1B-1D), or those expressing both *EGFP* and
554 *GFP-IR* (Figure 4B), as 100.
555
556 **Egg-to-adult viability of flies**
557 Mated female flies were placed on grape juice agar with yeast paste for 24
558 hours. Eggs were collected from the surface of the grape juice agar, and the number of
559 eggs were counted and placed on new standard fly food. After eclosion, the number of
560 adult flies was counted. Egg-to-adult viability was calculated by dividing the number of
561 adult flies by the number of eggs. More than 500 eggs per genotype were used. Data
562 were normalized by setting the values of samples from flies expressing two copies of
563 EGFP as 100 (Fig 2D).
564
565 **Climbing assay**
566 Twenty male flies were gently introduced into a glass vial. After a 5-minute
567 adaptation period, the bottom of the vial was gently tapped and the height the flies
568 reached in 10 seconds was recorded using a digital video camera, and scored as follows:
569 0 (lower than 2 cm), 1 (from 2 to 3.9 cm), 2 (from 4 to 5.9 cm), 3 (from 6 to 7.9 cm), 4
570 (from 8 to 9.9 cm), and 5 (higher than 10 cm). Five trials were performed in each
571 experiment at intervals of 20 sec. The assay was performed between 8:00 and 10:00.
572 Climbing scores were calculated as an average of five trials.
573
574 **GeneSwitch experiments**
575 Flies were crossed in the absence of RU486 (mifepristone) on standard fly food.

576 One-day old adult male flies were transferred to Formula 4-24® Instant Drosophila
577 medium (Wako) with RU486 (100 μg/mL) for the indicated periods. Every 2 or 3 days,
578 flies were transferred to new medium with RU486. Climbing assays were performed at
579 0, 7, and 14 days after the start of RU486 treatment (Figure 2E).
580
581 **RNA fluorescence in situ hybridization**
582 Female third instar larvae were dissected in ice-cold phosphate-buffered saline
583 (PBS). Salivary glands were fixed with 4% paraformaldehyde (PFA) (pH 7.0) in PBS
584 for 30 min, and incubated in 100% methanol. Fixed samples were rehydrated in 75%
585 (v/v), 50%, and 25% ethanol in PBS, and rinsed in PBS and distilled water (DW).
586 Samples were then treated with 0.2 N HCl/DW for 20 min at room temperature (RT),
587 and rinsed in DW. Next, the samples were permeabilized with 0.2% Triton X-100 in
588 PBS for 10 min, rinsed in PBS for 5 min, fixed again in 4% PFA in PBS for 20 min,
589 then washed twice for 5 min each in PBS, and incubated twice for 15 min each in 2
590 mg/mL glycine/PBS. After the acetylation treatment, samples were incubated for 1 hour
591 at 37 °C in hybridization buffer consisting of 50% formamide, 2 × saline sodium citrate
592 (SSC), 0.2 mg/mL yeast tRNA, and 0.5 mg/mL heparin. For hybridization, samples
593 were incubated overnight at 80 °C with a 5′ end Alexa594-labeled $(G_2C_4)_4$ or Alexa488-
594 labeled $(C_2G_4)_4$ locked nucleic acid (LNA) probe (5 nM) in hybridization buffer. These
595 LNA probes were synthesized by GeneDesign Inc. After the hybridization, samples
596 were washed once for 5 min in 4 × SSC at 80 °C, three times for 20 min each in 2 × SSC
597 and 50% formamide at 80 °C, three times for 40 min each in 0.1 × SSC at 80 °C, and
598 once for 5 min in PBS containing 0.5% Triton X-100 (PBT) at RT. Nuclei were stained
599 with 4',6-diamidino-2-phenylindole (DAPI) or 2'-(4-ethoxyphenyl)-5-(4-methyl-1-

600 piperazinyl)-2,5'-bi-1-*H*-benzimidazole, trihydrochloride (Hoechst 33342). Stained
601 samples were mounted in SlowFade® Gold antifade reagent (Thermo Fisher Scientific)
602 and observed under a Zeiss LSM710 or LSM880 confocal laser-scanning microscope.
603 After RNA FISH, samples were scanned using a Zeiss LSM710 or LSM880
604 confocal laser-scanning microscope along the z-axis direction. One z-stack image was
605 taken per salivary gland using ZEN imaging software (Zeiss). RNA foci-positive nuclei
606 in more than 30 cells per salivary gland were counted, and the percentage of nuclei
607 containing RNA foci in the salivary gland was calculated. Ten salivary glands were
608 analyzed for each genotype.
609
610 **Immunohistochemistry**
611 Female third instar larvae were dissected in ice-cold PBS. Eye imaginal discs
612 and salivary glands were fixed with 4% PFA in PBS for 30 min and washed 3 times
613 with PBT. After blocking with 5% goat serum/PBT, the samples were incubated
614 overnight at 4 °C with a rat monoclonal anti-poly(GR) antibody (clone 5A2,
615 MABN778, Millipore), a rabbit polyclonal anti-poly(GA) antibody (CAC-TIP-C9-P01,
616 Cosmo Bio), a rabbit polyclonal anti-poly(GP) antibody (NBP2-25018, Novus
617 Biologicals), or a rabbit polyclonal anti-FUS antibody (A300-302A, Bethyl
618 Laboratories) at 1:1,000 dilution as the primary antibody. After washing 3 times with
619 PBT, the samples were incubated with an Alexa 633-conjugated anti-rat antibody (A-
620 21094, Thermo Fisher Scientific), or an Alexa 488-conjugated or Alexa 555-conjugated
621 anti-rabbit antibody (A-11008 or A-21428, respectively, Thermo Fisher Scientific) at
622 1:500 dilution as the secondary antibody. After washing 3 times with PBT, nuclei were
623 stained with DAPI or Hoechst 33342. Stained samples were mounted in SlowFade®

624 Gold antifade reagent and observed using a Zeiss LSM710 or LSM880 confocal laser-
625 scanning microscope.
626 The number of DPR aggregates in the eye discs was quantitatively measured
627 using ZEN imaging software (Zeiss), as follows: 1) selection of photoreceptor neurons
628 within the 13 developing ommatidia in rows 2 and 3 at the posterior end of the eye discs
629 (Saitoh et al., 2015) by DAPI or Hoechst 33342 staining, because these ommatidia are
630 at similar stages of development and can be easily identified; 2) counting of the number
631 of DPR aggregates with a diameter of larger than 2 μm in the cytoplasm. Ten to 15 eye
632 discs were analyzed for each genotype.
633
634 **Measurement of poly(GP) protein levels**
635 The heads of 5-day-old female flies expressing both $(G_4C_2)_{89}$(H) and either
636 *EGFP*, *FUS*, or *FUS-RRMmut* using the *GMR-Gal4* driver were collected and stored at
637 –80 °C. Samples were prepared using a previously reported method (Tran et al., 2015).
638 Poly(GP) levels were measured by a sandwich immunoassay that uses Meso Scale
639 Discovery electrochemiluminescence detection technology, as described previously (Su
640 et al., 2014). Data were normalized by setting the values of samples from flies
641 expressing $(G_4C_2)_{89}$(H) and *EGFP* (Figure 3F) as 100.
642
643 **Western blotting**
644 To assess the expression levels of FUS and FUS-RRMmut (Figure 2—figure
645 supplement 1), or GR-GFP (Figures 3G–3I), 10 heads of 5-day-old female flies
646 expressing *FUS* or *FUS-RRMmut*, or both *LDS*-$(G_4C_2)_{44}^{\text{GR-GFP}}$ and either *FUS* or *FUS-*
647 *RRMmut* using the *GMR-Gal4* driver were homogenized in 100 μL of sodium dodecyl

648 sulfate (SDS) sample buffer using a pestle, boiled for 5 min, and centrifuged at
649 10,000 × *g* for 3 min at 25 °C. Five μL of each supernatant were run on a 5% to 20%
650 gradient polyacrylamide gel (Wako) and then transferred onto an Immun-Blot®
651 polyvinylidene fluoride membrane (Bio-Rad). Membranes were blocked with 5% skim
652 milk in PBS containing 0.1% Tween-20 (PBST) or PVDF Blocking Reagent for Can
653 Get Signal® (TOYOBO) for 2 hours at RT, and then incubated overnight at 4 °C with a
654 rabbit polyclonal anti-FUS antibody (A300-302A, Bethyl Laboratories), a rat
655 monoclonal anti-poly(GR) antibody (clone 5A2, MABN778, Millipore), a Living
656 Colors® EGFP mouse monoclonal antibody (632569, Clontech), or a mouse monoclonal
657 anti-actin antibody (clone AC-40, A4700, Sigma-Aldrich) at 1:1,000 dilution as the
658 primary antibody. After washing 3 times with PBST, membranes were incubated for 2
659 hours at RT with either HRP-conjugated anti-rat, anti-rabbit, or anti-mouse antibody
660 (31470, 31460, or 31430, respectively, Invitrogen) at 1:5,000 dilution as the secondary
661 antibody, washed 3 times with PBST, treated with SuperSignal™ West Dura
662 chemiluminescent substrate (Thermo Fisher Scientific), and imaged using the
663 LuminoGraphII imaging system (ATTO). Data were normalized by setting the average
664 values of samples from flies expressing *FUS* (Figure 2—figure supplement 1B), or
665 those expressing both *LDS*-$(G_4C_2)_{44}^{\text{GR-GFP}}$ and *DsRed* as 100 (Figures 3H and 3I).
666

667 **Filter binding assay**

668 For preparation of FUS proteins with an N-terminal His tag (His-FUS), cDNAs
669 of the human FUS protein (wild type or RRM mutant) from pUAST-*FUS* or pUAST-
670 *FUS-RRMmut* were cloned into the multiple cloning site (*Xho*I and *Bam*HI) of the
671 plasmid vector pET-15b (Novagen) (Nomura et al., 2014). After transfection of the

plasmids into *E. coli* BL21 (DE3), the expression of His-FUS proteins was induced by culturing the transformed cells in the presence of 0.5 mM isopropyl β-*D*-thiogalactopyranoside (IPTG) at 20 °C for 20 hours. Cells were lysed by ultrasonication in PBS (pH 7.4) containing 2% (v/v) Triton X-100, 1 M NaCl, DNase I, $MgSO_4$, and ethylenediaminetetraacetic acid-free Complete Protease Inhibitor Cocktail (Roche Applied Science). After centrifugation at 20,000 × *g* for 30 min at 4 °C, the pellets were redissolved in a buffer (pH 7.0) containing 6 M guanidine hydrochloride (GdnHCl), 50 mM Tris, and 1 M NaCl. His-FUS proteins in the pellets were purified by Ni^{2+} affinity chromatography. In brief, the His-FUS proteins were mixed with Profinity IMAC Ni^{2+}-charged resin (Bio-Rad) for 30 min at 20 °C. Then, FUS proteins bound to the resin were washed with wash buffer (6 M GdnHCl, 50 mM Tris, and 1 M NaCl, pH 7.0), and eluted with elution buffer (6 M GdnHCl, 50 mM Tris, 100 mM NaCl, and 250 mM imidazole, pH 7.0). For preparation of soluble, refolded FUS, FUS proteins (200 μM) in the elution buffer were diluted 20-fold with a buffer (pH 7.0) containing 50 mM Tris, 100 mM NaCl, 10% (v/v) glycerol, and 5 mM Tris (2-carboxyethyl) phosphine (buffer A), which, however, produced significant amounts of precipitate. This insoluble material was removed by centrifugation at 20,000 × *g* for 10 min at 4 °C, resulting in the recovery of soluble FUS proteins in the supernatant fraction. Protein concentrations were spectroscopically determined from the absorbance at 280 nm using the following extinction coefficients: 71,630 cm^{-1} M^{-1} for both FUS and FUS-RRMmut.

Biotinylated RNAs were synthesized by GeneDesign Inc. Ten nM biotin-$(G_4C_2)_4$, 10 nM biotin-$(AAAAAA)_4$, or 10 nM biotin-$(UUAGGG)_4$ (telomeric repeat-containing RNA: TERRA) were incubated with soluble FUS proteins (5, 10, or 50 nM) in buffer A with 0.4 U/μL RNase inhibitor (RNasin Plus RNase Inhibitor, Promega).

696 Biotinylated $(AAAAAA)_4$ and TERRA are negative and positive controls, respectively.
697 After an hour at RT, the mixture was filtered through a nitrocellulose membrane
698 (PROTRAN®, 0.2 μm, Amersham Biosciences) overlaid on a nylon membrane
699 (Hybond-N^+, 0.45 μm, Schleicher & Schuell) in a 96-well slot-blot apparatus (ATTO)
700 (Furukawa et al., 2011). After extensive washing of the membranes with buffer A, the
701 bound RNAs were crosslinked to the membranes using ultraviolet radiation (254 nm;
702 UV Stratalinker, Stratagene) at an energy level of 0.12 J. After blocking with 3% (w/v)
703 BSA in tris-buffered saline with 0.1% Tween-20, the membranes were incubated with
704 streptavidin-HRP (1:5,000; Nacalai Tesque), and the biotinylated RNAs on the
705 membranes were detected with ImmunoStar LD reagent (Wako).
706
707 **Preparation of recombinant FUS protein**
708 For preparation of the FUS protein, the human *FUS* (WT) gene flanked at the 5′
709 end with an *Nde*I recognition site and at the 3′ end with a *Xho*I recognition site was
710 amplified by PCR from pUAST-*FUS*. PCR fragments were digested with *Nde*I and
711 *Xho*I. These fragments were ligated into the cloning sites of the plasmid vector pET-21b
712 (Novagen) between *Nde*I and *Xho*I. After transfection of the plasmids into *E. coli* BL21
713 (DE3), expression of the FUS protein was induced by culturing the transformed cells in
714 the presence of 0.5 mM IPTG at 37 °C for 6 hours. Cells were harvested by
715 centrifugation and suspended with buffer B (10% glycerol, 20 mM 4-(2-hydroxyethyl)-
716 1-piperazineethanesulfonic acid [HEPES]-NaOH [pH 7.0], 300 mM NaCl, 1 mM
717 dithiothreitol [DTT], 1 mM ethylenediaminetetraacetic acid [EDTA], 0.1% Tween-20,
718 and 0.1% benzamidine hydrochloride) containing 1.5 mg/mL lysozyme, and stored for
719 30 min on ice. Cell lysates were sonicated, and insoluble protein was collected by

720 centrifugation. The pellet was solubilized in buffer C (6 M urea, 10% glycerol, 20 mM
721 HEPES-NaOH [pH 7.0], 1 mM DTT, 1 mM EDTA, and 0.1% benzamidine
722 hydrochloride). After centrifugation, supernatants were loaded onto a DE52 (GE
723 Healthcare) open column. The flow-through fraction was loaded onto a CM52 (GE
724 Healthcare) open column. The flow-through fraction of DE52 was applied to a CAPTO
725 S column (GE Healthcare), and the flow-through fraction was collected using the
726 ÄKTAexplorer 10S/100 system (GE Healthcare). The flow-through fraction was applied
727 to a Mono S column (GE Healthcare). Proteins were fractionated with a 0 to 500 mM
728 linear gradient of NaCl in buffer D (6 M urea, 10% glycerol, 20 mM HEPES-NaOH
729 [pH 7.0], 1 mM DTT, and 1 mM EDTA) using ÄKTA explorer 10 S/100 system. The
730 FUS fraction was eluted at 150 to 200 mM NaCl. For refolding, the eluted peak fraction
731 was diluted fivefold using refolding buffer (900 mM arginine, 100 mM N-cyclohexyl-2-
732 hydroxyl-3-aminopropanesulfonic acid [pH 9.5], 0.3 mM reduced glutathione, 0.03 mM
733 oxidized glutathione, and 1 mM $ZnCl_2$), and stored overnight at RT. The solution was
734 concentrated using a centrifugal filter (Vivaspin 6-10 kDa; GE Healthcare) to 1 to 2
735 mg/mL, and then dialyzed against buffer E (10% glycerol, 20 mM HEPES-NaOH [pH
736 6.8], 300 mM NaCl, 0.1 mM EDTA, and 10 mM β-cyclodextrin), and stored frozen at
737 −80 °C.
738
739 **Surface plasmon resonance analyses**
740 The binding of FUS to $(G_4C_2)_4$ RNA was analyzed using a Biacore T200
741 instrument (GE Healthcare). $(G_4C_2)_4$ RNAs biotinylated at the 5′ end in 10 mM HEPES
742 pH 6.8 and 500 mM MCl (M = K, Na, or Li) was injected over the streptavidin-coated
743 surface of a sensor chip SA (GE Healthcare). The amount of immobilized RNA was as

744 follows: 240 resonance unit (RU) in KCl, 363 RU in NaCl, or 319 RU in LiCl buffer
745 condition. Binding experiments were performed using the single cycle kinetics method.
746 The running buffer used was 20 mM HEPES (pH 6.8), 1 mM $MgCl_2$, 0.05% Tween-20,
747 and 150 mM KCl, NaCl, or LiCl. FUS was diluted in the running buffer and injected
748 sequentially over the RNA-immobilized sensor surface in increasing concentrations
749 (0.016, 0.031, 0.063, 0.13, or 0.25 μM). Sensorgrams were obtained at 25 °C, 30
750 μL/min flow rate, 60 seconds of contact time, and 120 seconds of dissociation time.
751
752 **Circular dichroism spectroscopy**
753 CD spectra were measured at 25 °C using a spectropolarimeter model J-820
754 (JASCO). $(G_4C_2)_4$ RNA was synthesized by GeneDesign Inc. and dissolved in 20 mM
755 HEPES (pH 6.8), 18.75 mM NaCl, 10 mM $MgCl_2$, 0.625% glycerol, 0.625 mM β-
756 cyclodextrin, and 0.0625 mM EDTA with 150 mM KCl, NaCl, or LiCl. RNA samples
757 containing 150 mM KCl were first heated at 95 °C for 5 min and then cooled to RT to
758 form the G-quadruplex structure. The other samples were not heated. FUS (1 μM) was
759 added to the RNA sample (4 μM) and mixed before recording the spectrum. CD spectra
760 were recorded at a speed of 50 nm min^{-1} and a resolution of 1 nm, and 10 scans were
761 averaged.
762
763 **Nuclear magnetic resonance spectroscopy**
764 All one-dimensional ^1H NMR spectral data were recorded using AVANCE III
765 800 MHz NMR spectrometers equipped with a TXI cryogenic probe (Bruker BioSpin)
766 at 25 °C. $(G_4C_2)_4$ RNA dissolved in 20 mM HEPES (pH 6.8), 150 mM KCl, 18.75 mM
767 NaCl, 10 mM $MgCl_2$, 0.625% glycerol, 0.625 mM β-cyclodextrin, and 0.0625 mM

768 EDTA was first heated at 95 °C for 5 min and then cooled to room temperature to form
769 the G-quadruplex structure. The RNA (10 μM) was mixed with FUS at molar ratios
770 (RNA:FUS) of 1:0, 1:0.2, 1:0.4, and 0:1. The samples were then prepared at a final
771 concentration of 10% D_2O before recording their spectra. ^1H NMR data were acquired
772 using simple single 90° hard-pulse excitations following solvent signal suppression with
773 a jump-and-return pulse scheme. Free induction decay data (1,600 points in total) were
774 collected by repeating the scans (2,600 times) with an interscan delay of 2.5 seconds.
775 All NMR data were processed using Topspin 3.6 software (Bruker BioSpin).
776
777 **RNA synthesis for in vitro translation**
778 For preparation of the C9-RAN reporter plasmid, the pEF6-*C9orf72* intron1-
779 $(G_4C_2)_{80}$ vector was digested with *HindIII* and *NotI* to obtain the fragment *C9orf72*
780 intron1-$(G_4C_2)_{80}$, and subcloned into the pcDNA™5/FRT vector (Thermo Fisher
781 Scientific). To add the T7 promoter upstream of the *C9orf72* intron 1 sequence in this
782 pcDNA™5/FRT-*C9orf72* intron1-$(G_4C_2)_{80}$ vector, a forward primer including T7
783 promoter sequences with the 5′-terminal region of *C9orf72* intron 1 flanked at the 5′ end
784 with an *HindIII* recognition site, and a reverse primer recognizing the 3′-terminal region
785 of *C9orf72* intron 1 sequences including a *BssHII* recognition site were designed, and
786 used to amplify a fragment containing *C9orf72* intron 1 with a T7 promoter by PCR.
787 Then, this fragment was subcloned into the pcDNA™5/FRT-*C9orf72* intron1-$(G_4C_2)_{80}$
788 vector digested by *HindIII* and *BssHII*. In addition to the T7 promoter, the Myc tag in
789 the GA frame downstream of $(G_4C_2)_{80}$ was introduced into this vector.
790 The reporter plasmids were linearized with *XbaI*. Linearized DNA was *in vitro*
791 transcribed using mMESSAGE mMACHINE™ T7 Transcription Kit (Invitrogen)

792 according to the manufacturer's instructions. T7 reactions were carried out at 37 °C for
793 2 hours, treated with TURBO™ DNaseI for 15 min at 37 °C to remove the DNA
794 template, and then polyadenylated with *E. coli* Poly-A Polymerase (NEB) for 1 hour at
795 37 °C. Synthesized mRNAs were purified by LiCl precipitation. The size and quality of
796 the synthesized mRNAs were verified on a denaturing RNA gel.
797
798 **In vitro translation assay**
799 mRNAs of *C9orf72* intron1-$(G_4C_2)_{80}$ with a Myc tag in the GA frame were *in*
800 *vitro* translated with Flexi® Rabbit Reticulocyte Lysate System (Promega) according to
801 the manufacturer's instructions. Translation reactions were performed with 10 ng/μL
802 mRNA and contained 30% rabbit reticulocyte lysate, 10 μM amino-acid mix minus
803 methionine, 10 μM amino-acid mix minus leucine, 0.5 mM MgOAc, 100 mM KCl, 0.8
804 U/μL Murine RNAse Inhibitor (NEB), and 100 ng/μL human tRNAs purified from
805 HeLa cells. FUS or BSA at each concentration (10, 100, and 1,000 μM) was added for
806 translation in the lysate. Samples were incubated at 30 °C for 90 min before termination
807 by incubation on ice. Ten μL of samples were analyzed by 13% SDS-polyacrylamide
808 gel electrophoresis and Western blotting using a mouse monoclonal anti-Myc tag
809 antibody (clone 4A6, Sigma-Aldrich) as the primary antibody.
810
811 **Quantification and statistical analysis**
812 Statistical parameters including the definitions and exact values of n (e.g.,
813 number of experiments, number of flies, number of eye imaginal discs, etc.),
814 distributions, and deviations are stated in the figures and corresponding figure legends.
815 Multiple comparison tests using one-way ANOVA with Tukey's post hoc analysis were

816 performed for Figures 1B–1E, 2B–2D, 3B, 3C, 3E, 3F, 3H, 3I, 4B, 4D, 6B, 6C, 6D,
817 Figure 1—figure supplements 1C and 1D, Figure 1—figure supplements 2B–2D, and
818 Figure 4—figure supplements 1B–1D, multiple comparison test using two-way repeated
819 measures ANOVA with Tukey's post hoc analysis was performed for Figure 2E, and the
820 unpaired *t*-test was used for Figures 4F, 4G, 4I, and Figure 2—figure supplement 1B.
821 Differences in means were considered statistically significant at $P < 0.05$. All statistical
822 analyses were performed using GraphPad Prism 8 software.

823 As the sample sizes used in the present study were similar to previous
824 publications (Freibaum et al., 2015; Goodman et al., 2019; Mizielinska et al., 2014; Xu
825 et al., 2013), statistical analyses were performed afterwards without interim data
826 analysis. Data were not excluded, and were collected and processed randomly. Sample
827 collection and analyses for the measurement of poly(GP) protein levels were performed
828 in a double-blind manner. Data collection and analyses for other experiments were not
829 performed in a blind manner regarding the conditions of the experiments.
830

Acknowledgements

We thank Drs E. Storkebaum (Radboud University), N. Bonini (University of Pennsylvania), and B. McCabe (École Polytechnique Fédérale de Lausanne) for kindly providing the *caz* mutant, *UAS-LDS-*$(G_4C_2)_{44}^{\text{GR-GFP}}$, and *UAS-FLAG-caz* and *UAS-FLAG-FUS* flies, respectively. We acknowledge Bloomington Drosophila Stock Center and Vienna Drosophila Resource Center for providing various fly stocks. We thank Drs H. Imataka and K. Machida (University of Hyogo) for kindly providing human tRNAs for *in vitro* translation. We also thank the members of our laboratory for helpful discussions, K. Yamamoto, E. Wakisaka, T. Yamashita, and A. Sugai for their technical assistance, Dr. H. Akiko Popiel for critical reading and English editing of the manuscript, and the Center for Medical Research and Education, Graduate School of Medicine, Osaka University for supplying experimental equipment. This work was supported by Grants-in-Aid for Scientific Research on Innovative Areas (Brain Protein Aging and Dementia Control) (17H05699 to Y.N. and 17H05705 to Y. Furukawa), Transformative Research Areas (A) (Multifaceted Proteins) (20H05927 to Y.N. and K.M.), and Strategic Research Program for Brain Sciences (11013026 to Y.N.), from the Ministry of Education, Culture, Sports, Science, and Technology, Japan; by Grants in-Aid for Scientific Research (B) (21H02840 to Y.N. and 20H03602 to K.M.), Scientific Research (C) (15K09331 and 19K07823 to M.U., 17K07291 to A.I.), Young Scientists (A) (17H05091 to K.M.), Young Scientists (B) (25860733 to M.U.), and Challenging Exploratory Research (24659438 to Y.N. and 18K19515 to K.M.) from the Japan Society for the Promotion of Science, Japan; by a Health Labor Sciences Research Grant for Research on Development of New Drugs (H24-Soyaku-Sogo-002 to Y.N.) from the Ministry of Health, Labor and Welfare, Japan; by grants for Strategic Research

855 Program for Brain Sciences (JP15dm0107026 and JP20dm0107061 to Y.N.), Practical
856 Research Projects for Rare/Intractable Diseases (JP16ek0109018, JP19ek0109222, and
857 JP20ek0109316 to Y.N.), and Platform Project for Supporting Drug Discovery and Life
858 Science Research [Basis for Supporting Innovative Drug Discovery and Life Science
859 Research] (JP19am0101072 to T.F.) from Japan Agency for Medical Research and
860 Development, Japan; Intramural Research Grants for Neurological and Psychiatric
861 Disorders (27-7, 27-9, 30-3, 30-9, and 3-9 to Y.N.) from the National Center of
862 Neurology and Psychiatry; an IBC Grant (H28 to Y.N.) from the Japan Amyotrophic
863 Lateral Sclerosis Association; grants from Takeda Science Foundation (2017 to M.U.
864 and 2016 to K.M.); and a grant from SENSHIN Medical Research Foundation (2018 to
865 K.M.).
866

867

868 **References**

869 Ash, P. E., Bieniek, K. F., Gendron, T. F., Caulfield, T., Lin, W. L., Dejesus-
870 Hernandez, M., van Blitterswijk, M. M., Jansen-West, K., Paul, J. W., 3rd, Rademakers,
871 R., Boylan, K. B., Dickson, D. W., and Petrucelli, L. (2013). Unconventional translation
872 of C9ORF72 GGGGCC expansion generates insoluble polypeptides specific to
873 c9FTD/ALS. Neuron *77*, 639–646. https://doi.org/10.1016/j.neuron.2013.02.004

874

875 Bajc Česnik, A., Darovic, S., Prpar Mihevc, S., Štalekar, M., Malnar, M.,
876 Motaln, H., Lee, Y. B., Mazej, J., Pohleven, J., Grosch, M., Modic, M., Fonovič, M.,
877 Turk, B., Drukker, M., Shaw, C. E., and Rogelj, B. (2019). Nuclear RNA foci from
878 C9ORF72 expansion mutation form paraspeckle-like bodies. J Cell Sci. *132*, jcs224303.
879 https://doi.org/10.1242/jcs.224303

880

881 Boivin, M., Pfister, V., Gaucherot, A., Ruffenach, F., Negroni, L., Sellier, C., and
882 Charlet-Berguerand, N. (2020). Reduced autophagy upon C9ORF72 loss synergizes
883 with dipeptide repeat protein toxicity in G4C2 repeat expansion disorders. EMBO J. *39*,
884 e100574. https://doi.org/10.15252/embj.2018100574

885

886 Celona, B., Dollen, J. V., Vatsavayai, S. C., Kashima, R., Johnson, J. R., Tang,
887 A. A., Hata, A., Miller, B. L., Huang, E. J., Krogan, N. J., Seeley, W. W., and Black, B.
888 L. (2017). Suppression of *C9orf72* RNA repeat-induced neurotoxicity by the ALS-
889 associated RNA-binding protein Zfp106. eLife *6*, e19032.
890 https://doi.org/10.7554/eLife.19032

Cheng, W., Wang, S., Mestre, A. A., Fu, C., Makarem, A., Xian, F., Hayes, L. R., Lopez-Gonzalez, R., Drenner, K., Jiang, J., Cleveland, D. W., and Sun, S. (2018). C9ORF72 GGGGCC repeat-associated non-AUG translation is upregulated by stress through eIF2α phosphorylation. Nat. Commun. *9*, 51. https://doi.org/10.1038/s41467-017-02495-z

Cheng, W., Wang, S., Zhang, Z., Morgens, D. W., Hayes, L. R., Lee, S., Portz, B., Xie, Y., Nguyen, B. V., Haney, M. S., Yan, S., Dong, D., Coyne, A. N., Yang, J., Xian, F., Cleveland, D. W., Qiu, Z., Rothstein, J. D., Shorter, J., Gao, F. B., Bassik, M.C., and Sun, S. (2019). CRISPR-Cas9 Screens Identify the RNA Helicase DDX3X as a Repressor of C9ORF72 (GGGGCC)n Repeat-Associated Non-AUG Translation. Neuron *104*, 885–898.e8. https://doi.org/10.1016/j.neuron.2019.09.003

Choi, S. Y., Lopez-Gonzalez, R., Krishnan, G., Phillips, H. L., Li, A. N., Seeley, W. W., Yao, W. D., Almeida, S., and Gao, F. B. (2019). C9ORF72-ALS/FTD-associated poly(GR) binds Atp5a1 and compromises mitochondrial function in vivo. Nat. Neurosci. *22*, 851–862. https://doi.org/10.1038/s41593-019-0397-0

Conlon, E. G., Lu, L., Sharma, A., Yamazaki, T., Tang, T., Shneider, N. A., and Manley, J. L. (2016). The C9ORF72 GGGGCC expansion forms RNA G-quadruplex inclusions and sequesters hnRNP H to disrupt splicing in ALS brains. eLife *5*, e17820. https://doi.org/10.7554/eLife.17820

Cooper-Knock, J., Walsh, M. J., Higginbottom, A., Robin Highley, J., Dickman, M. J., Edbauer, D., Ince, P. G., Wharton, S. B., Wilson, S. A., Kirby, J., Hautbergue, G. M., and Shaw, P. J. (2014). Sequestration of multiple RNA recognition motif-containing proteins by C9orf72 repeat expansions. Brain *137*, 2040–2051. https://doi.org/10.1093/brain/awu120

Daigle, J. G., Lanson, N. A., Jr, Smith, R. B., Casci, I., Maltare, A., Monaghan, J., Nichols, C. D., Kryndushkin, D., Shewmaker, F., and Pandey, U. B. (2013). RNA-binding ability of FUS regulates neurodegeneration, cytoplasmic mislocalization and incorporation into stress granules associated with FUS carrying ALS-linked mutations. Hum. Mol. Genet. *22*, 1193–1205. https://doi.org/10.1093/hmg/dds526

DeJesus-Hernandez, M., Mackenzie, I. R., Boeve, B. F., Boxer, A. L., Baker, M., Rutherford, N. J., Nicholson, A. M., Finch, N. A., Flynn, H., Adamson, J., Kouri, N., Wojtas, A., Sengdy, P., Hsiung, G. Y., Karydas, A., Seeley, W. W., Josephs, K. A., Coppola, G., Geschwind, D. H., Wszolek, Z. K., Feldman, H., Knopman, D.S., Petersen, R.C., Miller, B. L., Dickson, D. W., Boylan, K. B., Graff-Radford, N. R., and Rademakers, R. (2011). Expanded GGGGCC hexanucleotide repeat in noncoding region of C9ORF72 causes chromosome 9p-linked FTD and ALS. *Neuron*, *72*(2), 245–256. https://doi.org/10.1016/j.neuron.2011.09.011 (2011). Expanded GGGGCC hexanucleotide repeat in noncoding region of C9ORF72 causes chromosome 9p-linked FTD and ALS. Neuron *72*, 245–256.

Donnelly, C. J., Zhang, P. W., Pham, J. T., Haeusler, A. R., Mistry, N. A.,

Vidensky, S., Daley, E. L., Poth, E. M., Hoover, B., Fines, D. M., Maragakis, N., Tienari, P. J., Petrucelli, L., Traynor, B. J., Wang, J., Rigo, F., Bennett, C. F., Blackshaw, S., Sattler, R., and Rothstein, J. D. (2013). RNA toxicity from the ALS/FTD C9ORF72 expansion is mitigated by antisense intervention. Neuron *80*, 415–428. https://doi.org/10.1016/j.neuron.2013.10.015

Dumas, L., Herviou, P., Dassi, E., Cammas, A., and Millevoi, S. (2021). G-Quadruplexes in RNA Biology: Recent Advances and Future Directions. Trends Biochem. Sci. *46*, 270–283. https://doi.org/10.1016/j.tibs.2020.11.001

Fratta, P., Mizielinska, S., Nicoll, A. J., Zloh, M., Fisher, E. M., Parkinson, G., and Isaacs, A. M. (2012). C9orf72 hexanucleotide repeat associated with amyotrophic lateral sclerosis and frontotemporal dementia forms RNA G-quadruplexes. Sci. Rep. *2*, 1016. https://doi.org/10.1038/srep01016

Freibaum, B. D., Lu, Y., Lopez-Gonzalez, R., Kim, N. C., Almeida, S., Lee, K. H., Badders, N., Valentine, M., Miller, B. L., Wong, P. C., Petrucelli, L., Kim, H. J., Gao, F. B., and Taylor, J. P. (2015). GGGGCC repeat expansion in C9orf72 compromises nucleocytoplasmic transport. Nature *525*, 129–133. https://doi.org/10.1038/nature14974

Frickenhaus, M., Wagner, M., Mallik, M., Catinozzi, M., and Storkebaum, E. (2015). Highly efficient cell-type-specific gene inactivation reveals a key function for the Drosophila FUS homolog cabeza in neurons. Sci. Rep. *5*, 9107.

https://doi.org/10.1038/srep09107

Furukawa, Y., Kaneko, K., Watanabe, S., Yamanaka, K., and Nukina, N. (2011). A seeding reaction recapitulates intracellular formation of Sarkosyl-insoluble transactivation response element (TAR) DNA-binding protein-43 inclusions. J. Biol. Chem. *286*, 18664–18672. https://doi.org/10.1074/jbc.M111.231209

Gendron, T. F., Bieniek, K. F., Zhang, Y. J., Jansen-West, K., Ash, P. E., Caulfield, T., Daughrity, L., Dunmore, J. H., Castanedes-Casey, M., Chew, J., et al. (2013). Antisense transcripts of the expanded C9ORF72 hexanucleotide repeat form nuclear RNA foci and undergo repeat-associated non-ATG translation in c9FTD/ALS. Acta Neuropathol. *126*, 829–844. https://doi.org/10.1007/s00401-013-1192-8

Gendron, T. F., Bieniek, K. F., Zhang, Y. J., Jansen-West, K., Ash, P. E., Caulfield, T., Daughrity, L., Dunmore, J. H., Castanedes-Casey, M., Chew, J., Cosio, D. M., van Blitterswijk, M., Lee, W. C., Rademakers, R., Boylan, K. B., Dickson, D. W., and Petrucelli, L. (2017). Poly(GP) proteins are a useful pharmacodynamic marker for C9ORF72-associated amyotrophic lateral sclerosis. Sci, Transl. Med. *9*, eaai7866. https://doi.org/10.1126/scitranslmed.aai7866

Gijselinck, I., Van Langenhove, T., van der Zee, J., Sleegers, K., Philtjens, S., Kleinberger, G., Janssens, J., Bettens, K., Van Cauwenberghe, C., Pereson, S., Engelborghs, S., Sieben, A., De Jonghe, P., Vandenberghe, R., Santens, P., De Bleecker, J., Maes, G., Bäumer, V., Dillen, L., Joris, G., Cuijt, I., Corsmit, E., Elinck E., Van

Dongen, J., Vermeulen, S., Van den Broeck, M., Vaerenberg, C., Mattheijssens, M., Peeters, K., Robberecht, W., Cras, P., Martin, J. J., De Deyn P. P., Cruts, M., and Van Broeckhoven, C. (2012). A C9orf72 promoter repeat expansion in a Flanders-Belgian cohort with disorders of the frontotemporal lobar degeneration-amyotrophic lateral sclerosis spectrum: a gene identification study. Lancet Neurol. *11*, 54–65.

Goodman, L. D., Prudencio, M., Kramer, N. J., Martinez-Ramirez, L. F., Srinivasan, A. R., Lan, M., Parisi, M. J., Zhu, Y., Chew, J., Cook, C. N., Berson, A., Gitler, A. D., Petrucelli, L., and Bonini, N. M. (2019). Toxic expanded GGGGCC repeat transcription is mediated by the PAF1 complex in C9orf72-associated FTD. Nat. Neurosci. *22*, 863–874. https://doi.org/10.1038/s41593-019-0396-1

Green, K. M., Glineburg, M. R., Kearse, M. G., Flores, B. N., Linsalata, A. E., Fedak, S. J., Goldstrohm, A. C., Barmada, S. J., and Todd, P. K. (2017). RAN translation at C9orf72-associated repeat expansions is selectively enhanced by the integrated stress response. Nat. Commun. *8*, 2005. https://doi.org/10.1038/s41467-017-02200-0

Haeusler, A. R., Donnelly, C. J., Periz, G., Simko, E. A., Shaw, P. G., Kim, M. S., Maragakis, N. J., Troncoso, J. C., Pandey, A., Sattler, R., Rothstein, J. D., and Wang, J. (2014). C9orf72 nucleotide repeat structures initiate molecular cascades of disease. Nature *507*, 195–200. https://doi.org/10.1038/nature13124

Hardin, C. C., Watson, T., Corregan, M., and Bailey, C. (1992). Cation-

1011 dependent transition between the quadruplex and Watson-Crick hairpin forms of
1012 d(CGCG3GCG). Biochemistry *31*, 833–841. https://doi.org/10.1021/bi00118a028
1013
1014 Hutten, S., Usluer, S., Bourgeois, B., Simonetti, F., Odeh, H. M., Fare, C. M.,
1015 Czuppa, M., Hruska-Plochan, M., Hofweber, M., Polymenidou, M., Shorter, J.,
1016 Edbauer, D., Madl, T., and Dormann, D. (2020). Nuclear Import Receptors Directly
1017 Bind to Arginine-Rich Dipeptide Repeat Proteins and Suppress Their Pathological
1018 Interactions. Cell Rep. *33*, 108538. https://doi.org/10.1016/j.celrep.2020.108538
1019
1020 Ishiguro, T., Sato, N., Ueyama, M., Fujikake, N., Sellier, C., Kanegami, A.,
1021 Tokuda, E., Zamiri, B., Gall-Duncan, T., Mirceta, M., Furukawa, Y., Yokota, T., Wada,
1022 K., Taylor, J. P., Pearson, C. E., Charlet-Berguerand, N., Mizusawa, H., Nagai, Y., and
1023 Ishikawa, K. (2017). Regulatory Role of RNA Chaperone TDP-43 for RNA Misfolding
1024 and Repeat-Associated Translation in SCA31. Neuron *94*, 108–124.e7.
1025 https://doi.org/10.1016/j.neuron.2017.02.046
1026
1027 Jovičić, A., Mertens, J., Boeynaems, S., Bogaert, E., Chai, N., Yamada, S. B.,
1028 Paul, J. W., 3rd, Sun, S., Herdy, J. R., Bieri, G., Kramer, N. J., Gage, F. H., Van Den
1029 Bosch, L., Robberecht, W., and Gitler, A. D. (2015). Modifiers of C9orf72 dipeptide
1030 repeat toxicity connect nucleocytoplasmic transport defects to FTD/ALS. Nat. Neurosci.
1031 *18*, 1226–1229. https://doi.org/10.1038/nn.4085
1032
1033 Krishnan, G., Raitcheva, D., Bartlett, D., Prudencio, M., McKenna-Yasek, D.
1034 M., Douthwright, C., Oskarsson, B. E., Ladha, S., King, O. D., Barmada, S. J., Miller, T.

M., Bowser, R., Watts, J. K., Petrucelli, L., Brown, R. H., Kankel, M. W., and Gao, F. B. (2022). Poly(GR) and poly(GA) in cerebrospinal fluid as potential biomarkers for C9ORF72-ALS/FTD. Nat. Commun. *13*, 2799. https://doi.org/10.1038/s41467-022-30387-4

Kanadia, R. N., Shin, J., Yuan, Y., Beattie, S. G., Wheeler, T. M., Thornton, C. A., and Swanson, M. S. (2006). Reversal of RNA missplicing and myotonia after muscleblind overexpression in a mouse poly(CUG) model for myotonic dystrophy. Proc. Natl. Acad. Sci. USA *103*, 11748–11753. https://doi.org/10.1073/pnas.0604970103

Kwan, T., and Thompson, S. R. (2019). Noncanonical Translation Initiation in Eukaryotes. Cold Spring Harb. Perspect. Biol. *11*, a032672. https://doi.org/10.1101/cshperspect.a032672

Kwon, I., Xiang, S., Kato, M., Wu, L., Theodoropoulos, P., Wang, T., Kim, J., Yun, J., Xie, Y., and McKnight, S. L. (2014). Poly-dipeptides encoded by the C9orf72 repeats bind nucleoli, impede RNA biogenesis, and kill cells. Science *345*, 1139–1145. https://doi.org/10.1126/science.1254917

Lagier-Tourenne, C., Polymenidou, M., and Cleveland, D. W. (2010). TDP-43 and FUS/TLS: emerging roles in RNA processing and neurodegeneration. Hum. Mol. Genet. *19*, R46–R64. https://doi.org/10.1093/hmg/ddq137

Lee, K. H., Zhang, P., Kim, H. J., Mitrea, D. M., Sarkar, M., Freibaum, B. D., Cika, J., Coughlin, M., Messing, J., Molliex, A., Maxwell, B. A., Kim, N. C., Temirov, J., Moore, J., Kolaitis, R. M., Shaw, T. I., Bai, B., Peng, J., Kriwacki, R. W., and Taylor, J. P. (2016). C9orf72 Dipeptide Repeats Impair the Assembly, Dynamics, and Function of Membrane-Less Organelles. Cell *167*, 774–788.e17. https://doi.org/10.1016/j.cell.2016.10.002

Lee, Y. B., Chen, H. J., Peres, J. N., Gomez-Deza, J., Attig, J., Stalekar, M., Troakes, C., Nishimura, A. L., Scotter, E. L., Vance, C., Adachi, Y., Sardone, V., Miller, J. W., Smith, B. N., Gallo, J. M., Ule, J., Hirth, F., Rogelj, B., Houart, C., and Shaw, C. E. (2013). Hexanucleotide repeats in ALS/FTD form length-dependent RNA foci, sequester RNA binding proteins, and are neurotoxic. Cell Rep. *5*, 1178–1186. https://doi.org/10.1016/j.celrep.2013.10.049

Lehmer, C., Oeckl, P., Weishaupt, J. H., Volk, A. E., Diehl-Schmid, J., Schroeter, M. L., Lauer, M., Kornhuber, J., Levin, J., Fassbender, K., Landwehrmeyer, B., Schludi, M. H., Arzberger, T., Kremmer, E., Flatley, A., Feederle, R., Steinacker, P., Weydt, P., Ludolph, A. C., Edbauer, D., and Otto, M. German Consortium for Frontotemporal Lobar Degeneration (2017). Poly-GP in cerebrospinal fluid links C9orf72-associated dipeptide repeat expression to the asymptomatic phase of ALS/FTD. EMBO Mol. Med. *9*, 859–868. https://doi.org/10.15252/emmm.201607486

Li, L. B., Yu, Z., Teng, X., and Bonini, N. M. (2008). RNA toxicity is a component of ataxin-3 degeneration in Drosophila. Nature *453*, 1107–1111.

https://doi.org/10.1038/nature06909

Lin, Y., Mori, E., Kato, M., Xiang, S., Wu, L., Kwon, I., and McKnight, S. L. (2016). Toxic PR Poly-Dipeptides Encoded by the C9orf72 Repeat Expansion Target LC Domain Polymers. Cell *167*, 789–802.e12. https://doi.org/10.1016/j.cell.2016.10.003

Liu, H., Lu, Y. N., Paul, T., Periz, G., Banco, M. T., Ferré-D'Amaré, A. R., Rothstein, J. D., Hayes, L. R., Myong, S., and Wang, J. (2021). A Helicase Unwinds Hexanucleotide Repeat RNA G-Quadruplexes and Facilitates Repeat-Associated Non-AUG Translation. J. Am. Chem. Soc. *143*, 7368–7379. https://doi.org/10.1021/jacs.1c00131

Maharana, S., Wang, J., Papadopoulos, D. K., Richter, D., Pozniakovsky, A., Poser, I., Bickle, M., Rizk, S., Guillén-Boixet, J., Franzmann, T. M., Jahnel, M., Marrone, L., Chang, Y. T., Sterneckert, J., Tomancak, P., Hyman, A. A., and Alberti, S. (2018). RNA buffers the phase separation behavior of prion-like RNA binding proteins. Science *360*, 918–921. https://doi.org/10.1126/science.aar7366

Malik, I., Kelley, C. P., Wang, E. T., and Todd, P. K. (2021). Molecular mechanisms underlying nucleotide repeat expansion disorders. Nat. Rev. Mol. Cell Biol. *22*, 589–607. https://doi.org/10.1038/s41580-021-00382-6

Mann, J. R., Gleixner, A. M., Mauna, J. C., Gomes, E., DeChellis-Marks, M. R.,

Needham, P. G., Copley, K. E., Hurtle, B., Portz, B., Pyles, N. J., Guo, L., Calder, C. B., Wills, Z. P., Pandey, U. B., Kofler, J. K., Brodsky, J. L., Thathiah, A., Shorter, J., and Donnelly, C. J. (2019). RNA Binding Antagonizes Neurotoxic Phase Transitions of TDP-43. Neuron *102*, 321–338.e8. https://doi.org/10.1016/j.neuron.2019.01.048

May, S., Hornburg, D., Schludi, M. H., Arzberger, T., Rentzsch, K., Schwenk, B. M., Grässer, F. A., Mori, K., Kremmer, E., Banzhaf-Strathmann, J., Mann, M., Meissner, F., and Edbauer, D. (2014). C9orf72 FTLD/ALS-associated Gly-Ala dipeptide repeat proteins cause neuronal toxicity and Unc119 sequestration. Acta Neuropathol. *128*, 485–503. https://doi.org/10.1007/s00401-014-1329-4

Mitra, I., Huang, B., Mousavi, N., Ma, N., Lamkin, M., Yanicky, R., Shleizer-Burko, S., Lohmueller, K. E., and Gymrek, M. (2021). Patterns of de novo tandem repeat mutations and their role in autism. Nature *589*, 246–250. https://doi.org/10.1038/s41586-020-03078-7

Mizielinska, S., Grönke, S., Niccoli, T., Ridler, C. E., Clayton, E. L., Devoy, A., Moens, T., Norona, F. E., Woollacott, I., Pietrzyk, J., Cleverley, K., Nicoll, A. J., Pickering-Brown, S., Dols, J., Cabecinha, M., Hendrich, O., Fratta, P., Fisher, E., Partridge, L., and Isaacs, A. M. (2014). C9orf72 repeat expansions cause neurodegeneration in Drosophila through arginine-rich proteins. Science *345*, 1192–1194. https://doi.org/10.1126/science.1256800

(Mori et al., 2013a)

Mori, K., Lammich, S., Mackenzie, I. R., Forné, I., Zilow, S., Kretzschmar, H., Edbauer, D., Janssens, J., Kleinberger, G., Cruts, M., Herms, J., Neumann, M., Van Broeckhoven, C., Arzberger, T., and Haass, C. (2013). hnRNP A3 binds to GGGGCC repeats and is a constituent of p62-positive/TDP43-negative inclusions in the hippocampus of patients with C9orf72 mutations. Acta Neuropathol. *125*, 413–423. https://doi.org/10.1007/s00401-013-1088-7

(Mori et al., 2013b)

Mori, K., Arzberger, T., Grässer, F. A., Gijselinck, I., May, S., Rentzsch, K., Weng, S. M., Schludi, M. H., van der Zee, J., Cruts, M., Van Broeckhoven, C., Kremmer, E., Kretzschmar, H. A., Haass, C., and Edbauer, D. (2013). Bidirectional transcripts of the expanded C9orf72 hexanucleotide repeat are translated into aggregating dipeptide repeat proteins. Acta Neuropathol. *126*, 881–893. https://doi.org/10.1007/s00401-013-1189-3

(Mori et al., 2013c)

Mori, K., Weng, S. M., Arzberger, T., May, S., Rentzsch, K., Kremmer, E., Schmid, B., Kretzschmar, H. A., Cruts, M., Van Broeckhoven, C., Haass, C., and Edbauer, D. (2013). The C9orf72 GGGGCC repeat is translated into aggregating dipeptide-repeat proteins in FTLD/ALS. Science *339*, 1335–1338. https://doi.org/10.1126/science.1232927

Mori, K., Gotoh, S., Yamashita, T., Uozumi, R., Kawabe, Y., Tagami, S., Kamp, F., Nuscher, B., Edbauer, D., Haass, C., Nagai, Y., and Ikeda, M. (2021). The porphyrin

1155 TMPyP4 inhibits elongation during the noncanonical translation of the FTLD/ALS-
1156 associated GGGGCC repeat in the C9orf72 gene. J. Biol. Chem. *297*, 101120.
1157 https://doi.org/10.1016/j.jbc.2021.101120
1158
1159 Nomura, T., Watanabe, S., Kaneko, K., Yamanaka, K., Nukina, N., and
1160 Furukawa, Y. (2014). Intranuclear aggregation of mutant FUS/TLS as a molecular
1161 pathomechanism of amyotrophic lateral sclerosis. J. Biol. Chem. *289*, 1192–1202.
1162 https://doi.org/10.1074/jbc.M113.516492
1163
1164 Ozdilek, B. A., Thompson, V. F., Ahmed, N. S., White, C. I., Batey, R. T., and
1165 Schwartz, J. C. (2017). Intrinsically disordered RGG/RG domains mediate degenerate
1166 specificity in RNA binding. Nucleic Acids Res. *45*, 7984–7996.
1167 https://doi.org/10.1093/nar/gkx460
1168
1169 Rajkowitsch, L., Chen, D., Stampfl, S., Semrad, K., Waldsich, C., Mayer, O.,
1170 Jantsch, M. F., Konrat, R., Bläsi, U., and Schroeder, R. (2007). RNA chaperones, RNA
1171 annealers and RNA helicases. RNA Biol. *4*, 118–130.
1172 https://doi.org/10.4161/rna.4.3.5445
1173
1174 Reddy, K., Zamiri, B., Stanley, S., Macgregor, R. B., Jr, and Pearson, C. E.
1175 (2013). The disease-associated r(GGGGCC)n repeat from the C9orf72 gene forms tract
1176 length-dependent uni- and multimolecular RNA G-quadruplex structures. J. Biol. Chem.
1177 *288*, 9860–9866. https://doi.org/10.1074/jbc.C113.452532
1178

1179 Renton, A.E., Majounie, E., Waite, A., Simón-Sánchez, J., Rollinson, S., Gibbs,
1180 J. R., Schymick, J. C., Laaksovirta, H., van Swieten, J. C., Myllykangas, L., Kalimo, H.,
1181 Paetau, A., Abramzon, Y., Remes, A. M., Kaganovich, A., Scholz, S. W., Duckworth, J.,
1182 Ding, J., Harmer, D. W., Hernandez, D. G., Johnson. J. O., Mok, K., Ryten, M.,
1183 Trabzuni, D., Guerreiro, R. J., Orrell, R. W., Neal, J., Murray, A., Pearson, J., Jansen, I.
1184 E., Sondervan, D., Seelaar, H., Blake, D., Young, K., Halliwell, N., Callister, J. B.,
1185 Toulson, G., Richardson, A., Gerhard, A., Snowden, J., Mann, D., Neary, D., Nalls, M.
1186 A., Peuralinna, T., Jansson, L., Isoviita, V. M., Kaivorinne, A. L., Hölttä-Vuori, M.,
1187 Ikonen, E., Sulkava, R., Benatar, M., Wuu, J., Chiò, A., Restagno, G., Borghero, G.,
1188 Sabatelli, M., Heckerman, D., Rogaeva, E., Zinman, L., Rothstein, J. D., Sendtner, M.,
1189 Drepper, C., Eichler, E. E., Alkan, C., Abdullaev, Z., Pack, S. D., Dutra, A., Pak, E.,
1190 Hardy, J., Singleton, A., Williams, N.M., Heutink, P., Pickering-Brown, S., Morris, H.
1191 R., Tienari, P. J., and Traynor, B. J.. ITALSGEN Consortium (2011). A hexanucleotide
1192 repeat expansion in C9ORF72 is the cause of chromosome 9p21-linked ALS-FTD.
1193 Neuron *72*, 257–268.
1194
1195 Rudich, P., Snoznik, C., Watkins, S. C., Monaghan, J., Pandey, U. B., and
1196 Lamitina, S. T. (2017). Nuclear localized C9orf72-associated arginine-containing
1197 dipeptides exhibit age-dependent toxicity in C. elegans. Hum. Mol. Genet. *26*, 4916–
1198 4928. https://doi.org/10.1093/hmg/ddx372
1199
1200 Saitoh, Y., Fujikake, N., Okamoto, Y., Popiel, H. A., Hatanaka, Y., Ueyama, M.,
1201 Suzuki, M., Gaumer, S., Murata, M., Wada, K., and Nagai, Y. (2015). p62 plays a
1202 protective role in the autophagic degradation of polyglutamine protein oligomers in

1203 polyglutamine disease model flies. J. Biol. Chem. *290*, 1442–1453.
1204 https://doi.org/10.1074/jbc.M114.590281
1205
1206 Simone, R., Balendra, R., Moens, T. G., Preza, E., Wilson, K. M., Heslegrave,
1207 A., Woodling, N. S., Niccoli, T., Gilbert-Jaramillo, J., Abdelkarim, S., Clayton, E. L.,
1208 Clarke, M., Konrad, M. T., Nicoll, A. J., Mitchell, J. S., Calvo, A., Chio, A., Houlden,
1209 H., Polke, J. M., Ismail, M. A., Stephens, C.E., Vo, T., Farahat, A. A., Wilson, W. D.,
1210 Boykin, D. W., Zetterberg, H., Partridge, L., Wray, S., Parkinson, G., Neidle, S., Patani,
1211 R., Fratta, P., and Isaacs, A. M. (2018). G-quadruplex-binding small molecules
1212 ameliorate C9orf72 FTD/ALS pathology in vitro and in vivo. EMBO Mol. Med. *10*,
1213 22–31. https://doi.org/10.15252/emmm.201707850
1214
1215 Shi, Y., Lin, S., Staats, K. A., Li, Y., Chang, W. H., Hung, S. T., Hendricks, E.,
1216 Linares, G. R., Wang, Y., Son, E. Y., Wen, X., Kisler, K., Wilkinson, B., Menendez, L.,
1217 Sugawara, T., Woolwine, P., Huang, M., Cowan, M. J., Ge, B., Koutsodendris, N.,
1218 Sandor K. P., Komberg, J., Vangoor, V. R., Senthilkumar, K., Hennes, V., Seah, C.,
1219 Nelson, A. R., Cheng, T. Y., Lee, S. J., August, P. R., Chen, J. A., Wisniewski, N.,
1220 Hanson-Smith, V., Belgard, T. G., Zhang, A., Coba, M., Grunseich, C., Ward, M. E., van
1221 den Berg, L. H., Pasterkamp, R. J., Trotti, D., Zlokovic, B. V., and Ichida, J. K. (2018).
1222 Haploinsufficiency leads to neurodegeneration in C9ORF72 ALS/FTD human induced
1223 motor neurons. Nat. Med. *24*, 313–325. https://doi.org/10.1038/nm.4490
1224
1225 Sofola, O. A., Jin, P., Qin, Y., Duan, R., Liu, H., de Haro, M., Nelson, D. L., and
1226 Botas, J. (2007). RNA-binding proteins hnRNP A2/B1 and CUGBP1 suppress fragile X

CGG premutation repeat-induced neurodegeneration in a Drosophila model of FXTAS. Neuron *55*, 565–571. https://doi.org/10.1016/j.neuron.2007.07.021

Sonobe, Y., Ghadge, G., Masaki, K., Sendoel, A., Fuchs, E., and Roos, R. P. (2018). Translation of dipeptide repeat proteins from the C9ORF72 expanded repeat is associated with cellular stress. Neurobiol. Dis. *116*, 155–165. https://doi.org/10.1016/j.nbd.2018.05.009

Su, Z., Zhang, Y., Gendron, T. F., Bauer, P. O., Chew, J., Yang, W. Y., Fostvedt, E., Jansen-West, K., Belzil, V. V., Desaro, P., Johnston, A., Overstreet, K., Oh, S. Y., Todd, P. K., Berry, J. D., Cudkowicz, M. E., Boeve, B. F., Dickson, D., Floeter, M. K., Traynor, B. J., Morelli, C., Ratti, A., Silani, V., Rademakers, R., Brown, R. H., Rothstein, J. D., Boylan, K. B., Petrucelli, L., and Disney, M. D. (2014). Discovery of a biomarker and lead small molecules to target r(GGGGCC)-associated defects in c9FTD/ALS. Neuron *83*, 1043–1050. https://doi.org/10.1016/j.neuron.2014.07.041

Tabet, R., Schaeffer, L., Freyermuth, F., Jambeau, M., Workman, M., Lee, C. Z., Lin, C. C., Jiang, J., Jansen-West, K., Abou-Hamdan, H., Désaubry, L., Gendron, T., Petrucelli, L., Martin, F., and Lagier-Tourenne, C. (2018). CUG initiation and frameshifting enable production of dipeptide repeat proteins from ALS/FTD C9ORF72 transcripts. Nat. Commun. *9*, 152. https://doi.org/10.1038/s41467-017-02643-5

Tran, H., Almeida, S., Moore, J., Gendron, T. F., Chalasani, U., Lu, Y., Du, X., Nickerson, J. A., Petrucelli, L., Weng, Z., and Gao, F. B. (2015). Differential Toxicity of

Nuclear RNA Foci versus Dipeptide Repeat Proteins in a Drosophila Model of C9ORF72 FTD/ALS. Neuron *87*, 1207–1214. https://doi.org/10.1016/j.neuron.2015.09.015

Trost, B., Engchuan, W., Nguyen, C. M., Thiruvahindrapuram, B., Dolzhenko, E., Backstrom, I., Mirceta, M., Mojarad, B. A., Yin, Y., Dov, A., Chandrakumar, I., Prasolava, T., Shum, N., Hamdan, O., Pellecchia, G., Howe, J. L., Whitney, J., Klee, E. W., Baheti, S., Amaral, D. G., Anagnostou, E., Elsabbagh, M., Fernandez, B. A., Hoang, N., Lewis, S., Liu, X., Sjaarda, C., Smith, I. M., Szatmari, P., Zwaigenbaum, L., Glazer, D., Hartley, D., Stewart, A. K., Eberle, M. A., Sato, N., Pearson, C.E., Scherer, S.W., and Yuen, R. (2020). Genome-wide detection of tandem DNA repeats that are expanded in autism. Nature *586*, 80–86. https://doi.org/10.1038/s41586-020-2579-z

Tseng, Y. J., Sandwith, S. N., Green, K. M., Chambers, A. E., Krans, A., Raimer, H. M., Sharlow, M. E., Reisinger, M. A., Richardson, A. E., Routh, E. D., Smaldino, M. A., Wang, Y. H., Vaughn, J. P., Todd, P. K., and Smaldino, P. J. (2021). The RNA helicase DHX36-G4R1 modulates C9orf72 GGGGCC hexanucleotide repeat-associated translation. J. Biol. Chem. *297*, 100914. https://doi.org/10.1016/j.jbc.2021.100914

Waite, A. J., Bäumer, D., East, S., Neal, J., Morris, H. R., Ansorge, O., and Blake, D. J. (2014). Reduced C9orf72 protein levels in frontal cortex of amyotrophic lateral sclerosis and frontotemporal degeneration brain with the C9ORF72 hexanucleotide repeat expansion. Neurobiol. Aging *35*, 1779.e5–1779.e13. https://doi.org/10.1016/j.neurobiolaging.2014.01.016

Wang, J. W., Brent, J. R., Tomlinson, A., Shneider, N. A., and McCabe, B. D. (2011). The ALS-associated proteins FUS and TDP-43 function together to affect Drosophila locomotion and life span. J. Clin. Invest. *121*, 4118–4126. https://doi.org/10.1172/JCI57883

Wang, Z. F., Ursu, A., Childs-Disney, J. L., Guertler, R., Yang, W. Y., Bernat, V., Rzuczek, S. G., Fuerst, R., Zhang, Y. J., Gendron, T. F., Yildirim, I., Dwyer, B. G., Rice, J. E., Petrucelli, L., and Disney, M. D. (2019). The Hairpin Form of r(G4C2)^{exp} in c9ALS/FTD Is Repeat-Associated Non-ATG Translated and a Target for Bioactive Small Molecules. Cell Chem. Biol. *26*, 179–190.e12. https://doi.org/10.1016/j.chembiol.2018.10.018

Wen, X., Tan, W., Westergard, T., Krishnamurthy, K., Markandaiah, S. S., Shi, Y., Lin, S., Shneider, N. A., Monaghan, J., Pandey, U. B., Pasinelli, P., Ichida, J. K., and Trotti, D. (2014). Antisense proline-arginine RAN dipeptides linked to C9ORF72-ALS/FTD form toxic nuclear aggregates that initiate in vitro and in vivo neuronal death. Neuron *84*, 1213–1225. https://doi.org/10.1016/j.neuron.2014.12.010

Xu, Z., Poidevin, M., Li, X., Li, Y., Shu, L., Nelson, D. L., Li, H., Hales, C. M., Gearing, M., Wingo, T. S., and Jin, P. (2013). Expanded GGGGCC repeat RNA associated with amyotrophic lateral sclerosis and frontotemporal dementia causes neurodegeneration. Proc. Natl. Acad. Sci. USA *110*, 7778–7783. https://doi.org/10.1073/pnas.1219643110

Yamaguchi, M., Hirose, F., Inoue, Y. H., Shiraki, M., Hayashi, Y., Nishi, Y., and Matsukage, A. (1999). Ectopic expression of human p53 inhibits entry into S phase and induces apoptosis in the Drosophila eye imaginal disc. Oncogene *18*, 6767–6775. https://doi.org/10.1038/sj.onc.1203113

Zhang, Y. J., Gendron, T. F., Grima, J. C., Sasaguri, H., Jansen-West, K., Xu, Y. F., Katzman, R. B., Gass, J., Murray, M. E., Shinohara, M., Lin, W. L., Garrett, A., Stankowski, J. N., Daughrity, L., Tong, J., Perkerson, E. A., Yue, M., Chew, J., Castanedes-Casey, M., Kurti, A., Wang, Z. S., Liesinger, A. M., Baker, J. D., Jiang, J., Lagier-Tourenne, C., Edbauer, D., Cleveland, D. W., Rademakers, R., Boylan, K. B., Bu, G., Link, C. D., Dickey, C. A., Rothstein, J. D., Dickson, D. W., Fryer, J. D., and Petrucelli, L. (2016). C9ORF72 poly(GA) aggregates sequester and impair HR23 and nucleocytoplasmic transport proteins. Nat. Neurosci. *19*, 668–677. https://doi.org/10.1038/nn.4272

Zhang, Y. J., Gendron, T. F., Ebbert, M., O'Raw, A. D., Yue, M., Jansen-West, K., Zhang, X., Prudencio, M., Chew, J., Cook, C. N., Daughrity, L. M., Tong, J., Song, Y., Pickles, S. R., Castanedes-Casey, M., Kurti, A., Rademakers, R., Oskarsson, B., Dickson, D. W., Hu, W., Gitler, A. D., Fryer, J. D., and Petrucelli, L. (2018). Poly(GR) impairs protein translation and stress granule dynamics in C9orf72-associated frontotemporal dementia and amyotrophic lateral sclerosis. Nat. Med. *24*, 1136–1142. https://doi.org/10.1038/s41591-018-0071-1

Zhu, Q., Jiang, J., Gendron, T. F., McAlonis-Downes, M., Jiang, L., Taylor, A., Diaz Garcia, S., Ghosh Dastidar, S., Rodriguez, M. J., King, P., Zhang, Y., La Spada, A. R., Xu, H., Petrucelli, L., Ravits, J., Da Cruz, S., Lagier-Tourenne, C., and Cleveland, D. W. (2020). Reduced C9ORF72 function exacerbates gain of toxicity from ALS/FTD-causing repeat expansion in C9orf72. Nat. Neurosci. *23*, 615–624. https://doi.org/10.1038/s41593-020-0619-5

Zu, T., Gibbens, B., Doty, N. S., Gomes-Pereira, M., Huguet, A., Stone, M. D., Margolis, J., Peterson, M., Markowski, T. W., Ingram, M. A., Nan, Z., Forster, C., Low, W. C., Schoser, B., Somia, N. V., Clark, H. B., Schmechel, S., Bitterman, P. B., Gourdon, G., Swanson, M. S., Moseley, M., and Ranum, L. P. (2011). Non-ATG-initiated translation directed by microsatellite expansions. Proc. Natl. Acad. Sci. USA *108*, 260–265. https://doi.org/10.1073/pnas.1013343108

Zu, T., Liu, Y., Bañez-Coronel, M., Reid, T., Pletnikova, O., Lewis, J., Miller, T. M., Harms, M. B., Falchook, A. E., Subramony, S. H., Ostrow, L. W., Rothstein, J. D., Troncoso, J. C., and Ranum, L. P. (2013). RAN proteins and RNA foci from antisense transcripts in C9ORF72 ALS and frontotemporal dementia. Proc. Natl. Acad. Sci. USA *110*, E4968–E4977. https://doi.org/10.1073/pnas.1315438110

Zu, T., Cleary, J. D., Liu, Y., Bañez-Coronel, M., Bubenik, J. L., Ayhan, F., Ashizawa, T., Xia, G., Clark, H. B., Yachnis, A. T., Swanson, M. S., and Ranum, L. (2017). RAN Translation Regulated by Muscleblind Proteins in Myotonic Dystrophy Type 2. Neuron *95*, 1292–1305.e5. https://doi.org/10.1016/j.neuron.2017.08.039

1347

Figure legends

Figure 1. Screening for RBPs that suppress G_4C_2 repeat-induced toxicity in C9-ALS/FTD flies.

(A) Light microscopic images of the eyes in flies expressing both $(G_4C_2)_{42\text{ or }89}$ and the indicated RBPs using the *GMR-Gal4* driver. Coexpression of *FUS*, *IGF2BP1*, or *hnRNPA2B* suppressed eye degeneration in both $(G_4C_2)_{42}$ and $(G_4C_2)_{89}$ flies, indicated by "Suppression (strong)". Coexpression of *hnRNPR*, *SAFB2*, *SF3B3*, *hnRNPA1*, or *hnRNPL* suppressed eye degeneration in either $(G_4C_2)_{42}$ or $(G_4C_2)_{89}$ flies, indicated by "Suppression (weak)" (see also Figure 1—source data 2). Scale bar: 100 μm. (B) Quantification of eye size in $(G_4C_2)_{89}$ flies coexpressing the indicated RBPs (n = 5). (C), (D) Quantification of eye pigmentation in $(G_4C_2)_{89}$ flies (C) or $(G_4C_2)_{42}$ flies (D) coexpressing the indicated RBPs (n = 5). (E) Expression levels of $(G_4C_2)_{89}$ RNA in flies expressing both $(G_4C_2)_{89}$ and the indicated RBPs using the *GMR-Gal4* driver (five independent experiments, n = 25 flies per genotype). The $(G_4C_2)_{89}$(H) fly line expresses $(G_4C_2)_{89}$ RNA at a high level (see also Figure 1—figure supplement 1). In (B–E), data are presented as the mean ± SEM; $P < 0.0001$, as assessed by one-way ANOVA; n.s.: not significant, $^{*}P < 0.05$, $^{**}P < 0.01$, and $^{***}P < 0.001$, as assessed by Tukey's post hoc analysis.

Figure 1–figure supplement 1. Characterization of C9-ALS/FTD flies.

(A) $(G_4C_2)_n$ constructs used in this study. These constructs do not include an ATG start codon downstream of the UAS sequence, and were expressed in a tissue-specific manner using the *GAL4-UAS* system. (B) Light microscopic images of the eyes in flies expressing $(G_4C_2)_n$ using the *GMR-Gal4* driver. Scale bar: 100 μm. (C) Expression

1372 levels of $(G_4C_2)_n$ RNAs in flies expressing $(G_4C_2)_n$ using the *GMR-Gal4* driver. Strong
1373 eye degeneration with decreased eye size and loss of pigmentation was observed in
1374 $(G_4C_2)_{42\text{ or }89}$ flies, but not in $(G_4C_2)_9$ flies. Eye degeneration was confirmed in $(G_4C_2)_{42}$
1375 and two $(G_4C_2)_{89}$ independent fly lines. Degree of eye degeneration in two $(G_4C_2)_{89}$ fly
1376 lines was expression-level dependent [(L) vs (H) in $(G_4C_2)_{89}$] (three independent
1377 experiments, n = 15 flies per each genotype). Expression of G_4C_2 repeat RNA of the
1378 sense transcripts but not that of the antisense transcripts was confirmed. (D) Climbing
1379 ability at 1 day of age in flies expressing $(G_4C_2)_n$ using the *elav-Gal4* driver. Flies
1380 expressing $(G_4C_2)_{89}$(H) in neurons showed lethality. Decreasing climbing ability was
1381 observed in $(G_4C_2)_{42\text{ or }89}$ flies compared with $(G_4C_2)_9$ flies (five independent
1382 experiments, n = 100 flies per each genotype). (E) FISH analyses of G_4C_2 repeat RNA
1383 in the salivary glands of fly larvae with two copies of *GMR-Gal4* and $(G_4C_2)_{9\text{ or }89}$ (red:
1384 G_4C_2 RNA; yellow: G_2C_4 RNA; blue [DAPI]: nuclei). RNA foci formation
1385 (arrowheads) of the sense transcripts but not that of the antisense transcripts was
1386 confirmed. RNA foci were observed in $(G_4C_2)_{89}$ flies, but not in $(G_4C_2)_9$ flies. Scale
1387 bars: 100 μm (low magnification) or 20 μm (high magnification). (F)
1388 Immunohistochemical analyses of DPRs stained with anti-DPR antibodies in the eye
1389 imaginal discs of fly larvae with two copies of *GMR-Gal4* and $(G_4C_2)_{9\text{ or }89}$ (magenta:
1390 poly(GR); orange: poly(GA); green: poly(GP); blue [DAPI]: nuclei). Expression and
1391 cytoplasmic aggregation (arrowheads) of three DPRs in $(G_4C_2)_{89}$ flies, but not in
1392 $(G_4C_2)_9$ flies, were confirmed. Scale bars: 50 μm (low magnification), 10 μm (middle
1393 magnification), and 5 μm (high magnification). In (B–F), L: low-expression line; H:
1394 high-expression line. In (C) and (D), data are presented as the mean ± SEM; $P < 0.0001$,
1395 as assessed by one-way ANOVA; n.s.: not significant, and $^{***}P < 0.001$, as assessed by

Tukey's post hoc analysis.

Figure 1–figure supplement 2. Coexpression of FUS suppresses G_4C_2 repeat-induced toxicity in flies expressing $(G_4C_2)_{89}$.

(A) Light microscopic images of the eyes in flies expressing both $(G_4C_2)_{42 \text{ or } 89}$ and *FUS* using the *GMR-Gal4* driver. *FUS-2* and *FUS-3* are different strains from that in Figure 1. Scale bar: 100 μm. (B) Quantification of the eye size in $(G_4C_2)_{89}$ flies of the indicated genotypes (n = 10). (C), (D) Quantification of eye pigmentation in $(G_4C_2)_{89}$ flies (C) or $(G_4C_2)_{42}$ flies (D) of the indicated genotypes (n = 10). In (B–D), data are presented as the mean ± SEM; $P < 0.0001$, as assessed by one-way ANOVA; $^{***}P < 0.001$, as assessed by Tukey's post hoc analysis.

Figure 2. FUS suppresses G_4C_2 repeat-induced toxicity via its RNA-binding activity.

(A) Light microscopic images of the eyes in flies expressing both $(G_4C_2)_{89}$ and either *FUS* or *FUS-RRMmut* using the *GMR-Gal4* driver. Scale bar: 100 μm. (B) Quantification of eye size in the flies of the indicated genotypes (n = 10). (C) Quantification of eye pigmentation in the flies of the indicated genotypes (n = 10). (D) Egg-to-adult viability in flies expressing both $(G_4C_2)_{42}$ and either *FUS* or *FUS-RRMmut* using the *GMR-Gal4* driver (> 500 flies per genotype). (E) Climbing ability in flies expressing both $(G_4C_2)_{42}$ and *FUS* using the *elav-GeneSwitch* driver (five independent experiments, n = 100 flies per each genotype). In (B–E), data are presented as the mean ± SEM. In (B) and (C), $P < 0.0001$, as assessed by one-way ANOVA; n.s.: not significant, and $^{***}P < 0.001$, as assessed by Tukey's post hoc analysis. In (D), n.s.: not

significant and $^{***}P < 0.001$, as assessed by Tukey's multiple comparison test using wholly significant difference. In (E), n.s.: not significant, $^{*}P < 0.05$, $^{**}P < 0.01$ and $^{***}P < 0.001$, as assessed by two-way repeated measures ANOVA with Tukey's post hoc analysis.

Figure 2–figure supplement 1. Western blot analysis showing expression levels of FUS and FUS-RRMmut proteins.

(A) Western blot analysis of the FUS and FUS-RRMmut proteins in the heads of adult flies expressing *EGFP, FUS* or *FUS-RRMmut* using the *GMR-Gal4* driver, with an anti-FUS antibody. The arrowhead indicates bands from the FUS and FUS-RRMmut proteins, whereas the asterisk indicates bands resulting from nonspecific antibody binding. (B) Quantification of the FUS and FUS-RRMmut proteins from the Western blot analysis in (A) (n = 3).

In (B), data are presented as the mean ± SEM; n.s.: not significant, as assessed by the unpaired *t*-test.

Figure 3. FUS suppresses RNA foci formation and RAN translation from G_4C_2 repeat RNA.

(A) FISH analyses of G_4C_2 repeat RNA in the salivary glands of fly larvae expressing both $(G_4C_2)_{89}$ and either *FUS* or *FUS-RRMmut* using two copies of the *GMR-Gal4* driver (red: G_4C_2 RNA; blue [DAPI]: nuclei). Arrowheads indicate RNA foci. Scale bar: 20 μm. (B) Quantification of the number of nuclei containing RNA foci from the FISH analyses in (A) (n = 10). (C) Expression levels of $(G_4C_2)_{89}$ RNA in fly larvae expressing both $(G_4C_2)_{89}$ and either *FUS* or *FUS-RRMmut* using the *GMR-Gal4* driver (10

independent experiments, n = 50 flies per each genotype). (D) Immunohistochemical analyses of DPRs stained with anti-DPR antibodies in the eye imaginal discs of fly larvae expressing both $(G_4C_2)_{89}$ and either *FUS* or *FUS-RRMmut* using two copies of the *GMR-Gal4* driver (magenta: poly(GR); orange: poly(GA); green: poly(GP); blue [DAPI]: nuclei). Arrowheads indicate cytoplasmic aggregates. Scale bars: 20 μm (low magnification) or 5 μm (high magnification). (E) Quantification of the number of DPR aggregates from the immunohistochemical analyses in (D) [n = 14 or 15 (GR), or 10 (GA or GP)]. (F) Immunoassay to determine poly(GP) levels in flies expressing both $(G_4C_2)_{89}$ and either *FUS* or *FUS-RRMmut* using the *GMR-Gal4* driver (three independent experiments, n = 30 flies per each genotype). (G) Western blot analysis of the heads of adult flies expressing both LDS-$(G_4C_2)_{44}^{\text{GR-GFP}}$ and any of *DsRed*, *FUS* or *FUS-RRMmut* using the *GMR-Gal4* driver, using either an anti-GFP (upper panel) or anti-GR antibody (middle panel). (H and I) Quantification of GR-GFP protein levels from the Western blot analysis in (G) (nine independent experiments, n = 90 flies per each genotype). In (B), (C), (E), (F), (H), and (I), data are presented as the mean ± SEM. In (B), (E), and (F), $P < 0.0001$, as assessed by one-way ANOVA; n.s.: not significant, $^{*}P < 0.05$, $^{**}P < 0.01$, and $^{***}P < 0.001$, as assessed by Tukey's post hoc analysis. In (C), $P = 0.452$, as assessed by one-way ANOVA; n.s.: not significant, as assessed by Tukey's post hoc analysis. In (H), $P = 0.0148$, as assessed by one-way ANOVA; n.s.: not significant and $^{*}P < 0.05$, as assessed by Tukey's post hoc analysis. In (I), $P = 0.0072$, as assessed by one-way ANOVA; n.s.: not significant and $^{*}P < 0.05$, as assessed by Tukey's post hoc analysis.

Figure 3–figure supplement 1. Overexpression of *FUS* does not suppress eye

degeneration in DPR-only flies expressing DPRs translated from non-G_4C_2 RNAs. Light microscopic images of the eyes in DPR-only flies coexpressing either the poly(GR) or poly(GA) protein, and either *FUS* or *FUS-RRMmut* using the *GMR-Gal4* driver. Overexpression of *FUS* did not suppress the eye degeneration in flies expressing either $(GR)_{36}$ or $(GR)_{100}$. Overexpression of *FUS* also caused mild eye degeneration in flies expressing EGFP, $(GA)_{36}$, or $(GA)_{100}$, likely due to FUS toxicity.

Figure 4. Reduction of endogenous *caz* expression enhances G_4C_2 repeat-induced toxicity, RNA foci formation, and DPR aggregation.

(A) Light microscopic images of the eyes in flies expressing $(G_4C_2)_{89}$ using the *GMR-Gal4* driver, with knockdown of *caz*. Scale bar: 100 μm. (B) Quantification of eye size in flies of the indicated genotypes shown in (A) (n = 10). (C) Light microscopic images of the eyes in flies expressing $(G_4C_2)_{89}$ using the *GMR-Gal4* driver, with a hemizygous deletion of *caz*. Scale bar: 100 μm. (D) Quantification of eye size in the flies of the indicated genotypes shown in (C) (n = 10). (E) FISH analyses of G_4C_2 repeat RNA in the salivary glands of fly larvae expressing $(G_4C_2)_{89}$ using the *GMR-Gal4* driver, with knockdown of *caz* (red: G_4C_2 RNA; blue [DAPI]: nuclei). Arrowheads indicate RNA foci. Scale bar: 20 μm. (F) Quantification of the number of nuclei containing RNA foci from the FISH analyses in (E) (n = 10). (G) Expression levels of $(G_4C_2)_{89}$ RNA in fly larvae expressing $(G_4C_2)_{89}$ using the *GMR-Gal4* driver, with knockdown of *caz* (four independent experiments, n = 20 flies per each genotype). (H) Immunohistochemical analyses of DPRs stained with anti-DPR antibodies in the eye imaginal discs of fly larvae expressing $(G_4C_2)_{89}$ using two copies of the *GMR-Gal4* driver, with the knockdown of *caz*. (magenta: poly(GR); orange: poly(GA); green: poly(GP); blue

1492 [DAPI]: nuclei). Arrowheads indicate cytoplasmic aggregates. Scale bars: 20 μm (low
1493 magnification) or 5 μm (high magnification). (I) Quantification of the number of DPR
1494 aggregates from the immunohistochemical analyses in (H) (n = 10). In (B), (D), (F), (G)
1495 and (I), data are presented as the mean ± SEM. In (B) and (D), $P < 0.0001$, as assessed
1496 by one-way ANOVA; $^{***}P < 0.001$, as assessed by Tukey's post hoc analysis. In (F), (G),
1497 and (I), n.s.: not significant, $^{*}P < 0.05$, $^{**}P < 0.01$, and $^{***}P < 0.001$, as assessed by the
1498 unpaired *t*-test.
1499

1500 **Figure 4–figure supplement 1. Endogenous *caz* is a functional homologue of *FUS***
1501 **for the suppression of G_4C_2 repeat-induced toxicity.**

1502 (A) Light microscopic images of the eyes in flies expressing both $(G_4C_2)_{42\text{ or }89}$ and
1503 either *caz* (*FLAG-caz*) or *FUS-4* (*FLAG-FUS*) using the *GMR-Gal4* driver. *FUS-4* is a
1504 different strain from those used in Figure 1 and Figure 1–figure supplement 2. Scale
1505 bar: 100 μm. (B) Quantification of the eye size in $(G_4C_2)_{89}$ flies of the indicated
1506 genotypes (n = 10). (C), (D) Quantification of eye pigmentation in $(G_4C_2)_{89}$ flies (C) or
1507 $(G_4C_2)_{42}$ flies (D) of the indicated genotypes (n = 10). In (B–D), data are presented as
1508 the mean ± SEM; $P < 0.0001$, as assessed by one-way ANOVA; n.s.: not significant,
1509 $^{*}P < 0.05$, $^{**}P < 0.01$,and $^{***}P < 0.001$, as assessed by Tukey's post hoc analysis.
1510

1511 **Figure 5. FUS directly binds to and modulates the G-quadruplex structure of G_4C_2**
1512 **repeat RNA, resulting in the suppression of RAN translation *in vitro***

1513 (A) Analysis of the binding of His-tagged FUS proteins to biotinylated $(G_4C_2)_4$ RNA by
1514 the filter binding assay. The nitrocellulose membrane (left) traps RNA-bound FUS
1515 proteins, whereas unbound RNAs are recovered on the nylon membrane (right), and

then the RNAs trapped on each of the membranes was probed with streptavidin-horseradish peroxidase (HRP). Biotinylated $(AAAAAA)_4$ and $(UUAGGG)_4$ were used as negative and positive controls, respectively. (B–D) CD spectra of $(G_4C_2)_4$ RNA incubated with or without FUS in the presence of 150 mM KCl (B), NaCl (C), or LiCl (D). The CD spectrum of FUS alone was subtracted from that of $(G_4C_2)_4$ RNA incubated with FUS. The original data are shown in Figure 5—figure supplements 2B-2D. (E) Schema of the template RNA containing the $(G_4C_2)_{80}$ sequence and 113 nucleotides of the 5′-flanking region of intron 1 of the human *C9orf72* G_4C_2 repeat sequence. A Myc tag in the GA frame was introduced downstream of the $(G_4C_2)_{80}$ repeat sequence. (F) Western blot analysis of samples from *in vitro* translation using rabbit reticulocyte lysate in the presence or absence of increasing concentrations of FUS or BSA. The GA-Myc fusion protein was detected by Western blotting using the anti-Myc antibody. Quantifications are shown below each band, using the condition in the absence of each protein as a reference.

Figure 5–figure supplement 1. FUS colocalizes with G_4C_2 RNA foci.

Combined FISH and immunohistochemical analyses of G_4C_2 repeat RNA and FUS in the salivary glands of flies expressing both $(G_4C_2)_{89}$ and *FUS* using two copies of the *GMR-Gal4* driver. Arrows indicate colocalization of FUS with RNA foci. Scale bar: 10 μm.

Figure 5–figure supplement 2. FUS modulates the G-quadruplex structure of G_4C_2 repeat RNA.

(A–C) CD spectra of $(G_4C_2)_4$ RNA incubated with or without FUS in the presence of

150 mM KCl (B), NaCl (C), or LiCl (D). CD spectra of $(G_4C_2)_4$ RNA alone (black), FUS alone (green), sum of $(G_4C_2)_4$ RNA and FUS (blue), and the spectra of their coincubation (magenta) are shown. FUS interacts with $(G_4C_2)_4$ RNA under KCl or NaCl buffer conditions. (D) Imino proton NMR spectra of $(G_4C_2)_4$ RNA incubated with increasing amounts of FUS in the presence of 150 mM KCl.

Figure 6. Identification of G-quadruplex-targeting RBPs that suppress G_4C_2 repeat-induced toxicity in C9-ALS/FTD flies.

(A) Light microscopic images of eyes in flies expressing both $(G_4C_2)_{89}$ and the indicated G-quadruplex-targeting RBPs using the *GMR-Gal4* driver. Scale bar: 100 μm. (B) Quantification of eye size in the flies of the indicated genotypes (n = 10). (C) Quantification of eye pigmentation in the flies of the indicated genotypes (n = 10). (D) Expression levels of $(G_4C_2)_{89}$ RNA in flies expressing both $(G_4C_2)_{89}$ and the indicated G-quadruplex-targeting RBPs using the *GMR-Gal4* driver (five independent experiments, n = 25 flies per each genotype). In (B–D), data are presented as the mean ± SEM; $P < 0.0001$, as assessed by one-way ANOVA; n.s.: not significant, $^{*}P < 0.05$, and $^{***}P < 0.001$, as assessed by Tukey's post hoc analysis.

1558 **Tables**

1559 **Table 1. Association (k_a) and dissociation (k_d) rate and dissociation constants (K_D)**

1560 **between FUS and $(G_4C_2)_4$ RNA in different buffers as assessed by SPR analysis.**

1561

Buffer	k_a ($M^{-1}s^{-1}$) × 10^6	k_d (s^{-1}) × 10^{-3}	K_D (M)
KCl	1.4	22	1.5×10^{-8}
NaCl	0.41	54	1.3×10^{-7}
LiCl	0.0018	25	1.4×10^{-5}

1562
1563

1564 **Source data files and supplementary files list**

1565 Figure 1—source data 1. RNA-binding proteins and their cDNA accession numbers
1566 screened in the genetic analyses in Figure 1.
1567
1568 Figure 1—source data 2. Summary of the genetic analyses in Figure 1.
1569
1570 Figure 1—source data 3. Statistical data related to Figures 1B, 1C, 1D, and 1E.
1571
1572 Figure 1—figure supplement 1−source data 1. Statistical data related to Figure 1—
1573 figure supplements 1C and 1D
1574
1575 Figure 1—figure supplement 2−source data 1. Statistical data related to Figure 1—
1576 figure supplement 2B, 2C and 2D
1577
1578 Figure 2—source data 1. Statistical data related to Figures 2B, 2C, 2D, and 2E.
1579
1580 Figure 2—figure supplement 1−source data 1. Statistical data related to Figure 2—
1581 figure supplement 1B
1582
1583 Figure 3−source data 1. Statistical data related to Figures 3B, 3C, 3E, 3F, 3H, and 3H
1584
1585 Figure 3−source data 2. Source data related to Figure 3G
1586

1587 Figure 4—source data 1. Statistical data related to Figures 4B, 4D, 4F, 4G and 4I.

1588

1589 Figure 4—figure supplement 1−source data 1. Statistical data related to Figure 4—

1590 figure supplements 1B, 1C, and 1D

1591

1592 Figure 5—source data 1. Source data related to Figure 5F

1593

1594 Figure 6—source data 1. RNA-binding proteins and their cDNA accession numbers

1595 screened in the genetic analyses in Figure 6.

1596

1597 Figure 6—source data 2. Statistical data related to Figures 6B, 6C, and 6D.

1598

1599 Supplementary file 1. Full genotypes of the fly lines and their cultured temperatures.

1600

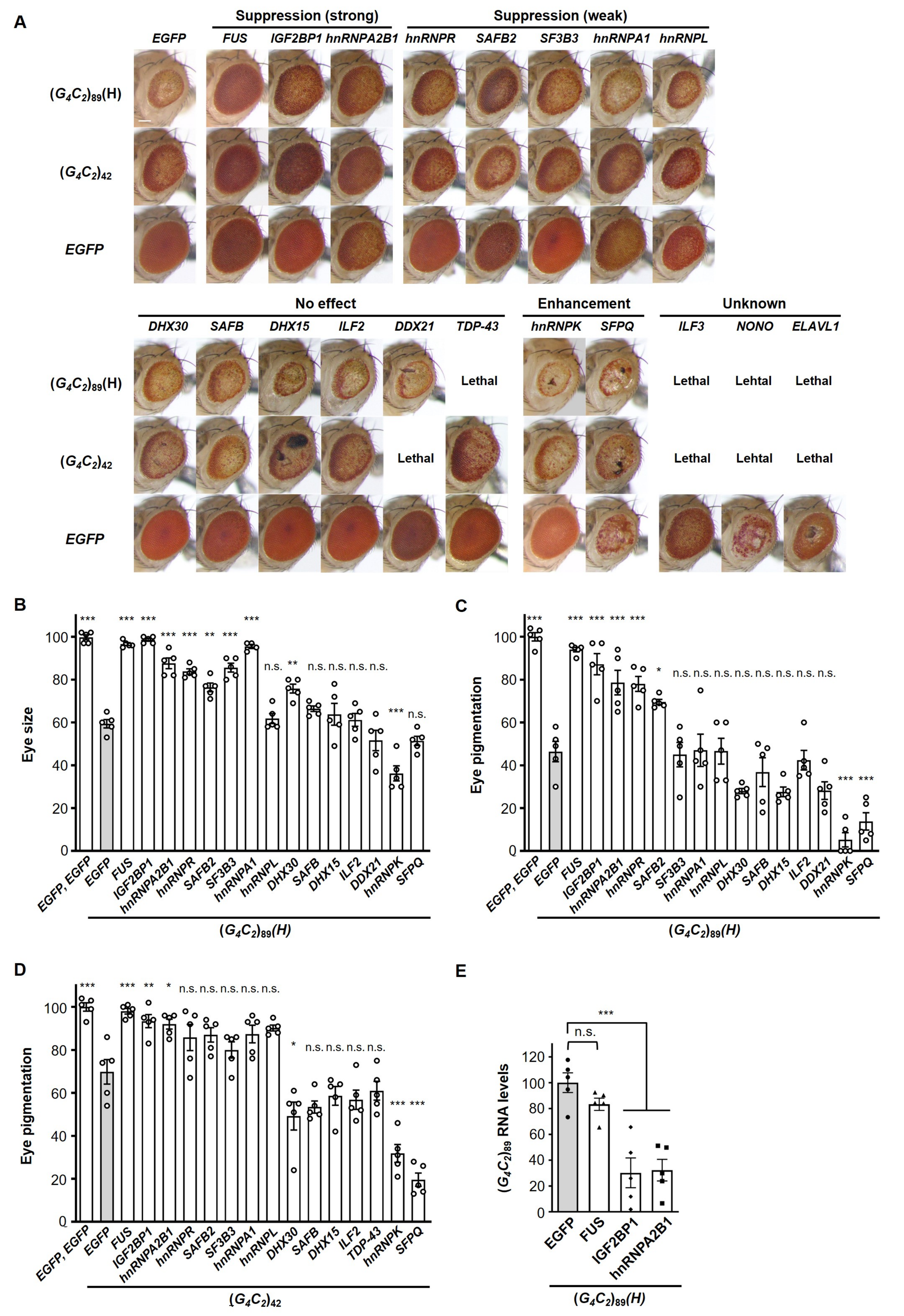
A
Suppression (strong)
Suppression (weak)
EGFP
FUS
IGF2BP1
hnRNPA2B1
hnRNPR
SAFB2
SF3B3
hnRNPA1
hnRNPL
(G4C2)89(H)
(G4C2)42
EGFP
No effect
Enhancement
Unknown
DHX30
SAFB
DHX15
ILF2
DDX21
TDP-43
hnRNPK
SFPQ
ILF3
NONO
ELAVL1
Lethal
Lehtal
B
Eye size
C
Eye pigmentation
D
Eye pigmentation
E
(G4C2)89 RNA levels
n.s.
(G4C2)42
(G4C2)89(H)

A

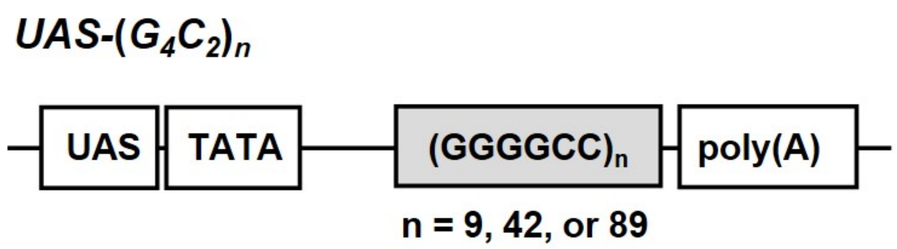
UAS-(G4C2)n
UAS
TATA
(GGGGCC)n
poly(A)
n = 9, 42, or 89

B

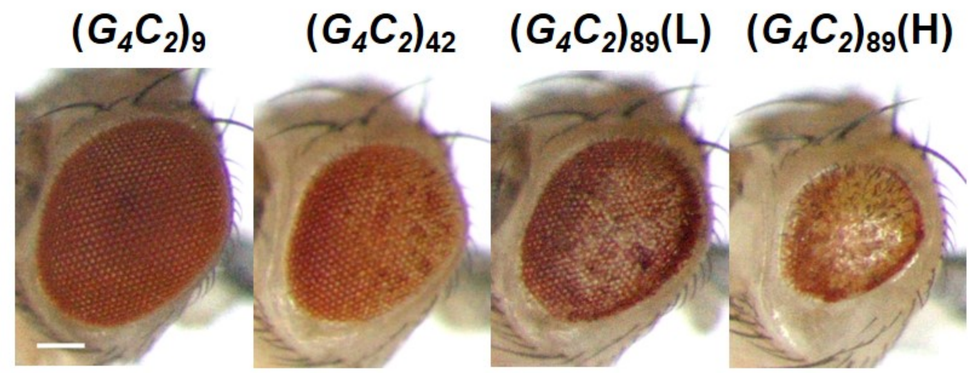
(G4C2)9
(G4C2)42
(G4C2)89(L)
(G4C2)89(H)

C

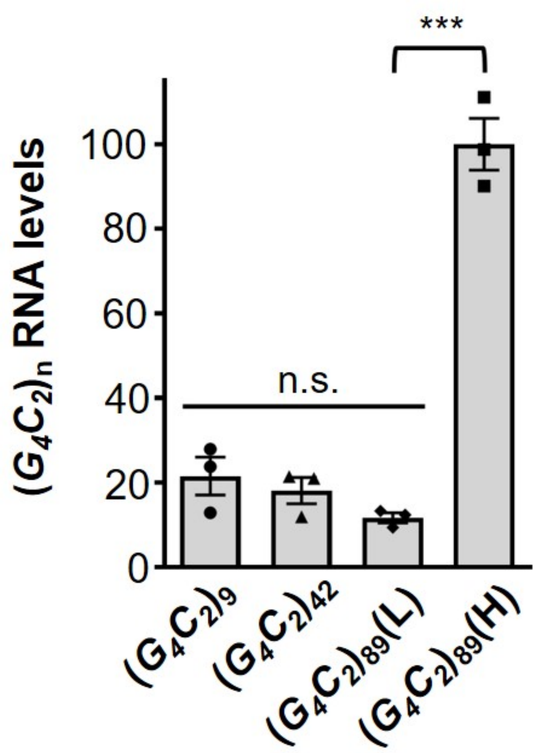
***
n.s.
(G4C2)n RNA levels
100
80
60
40
20
0
(G4C2)9
(G4C2)42
(G4C2)89(L)
(G4C2)89(H)

D

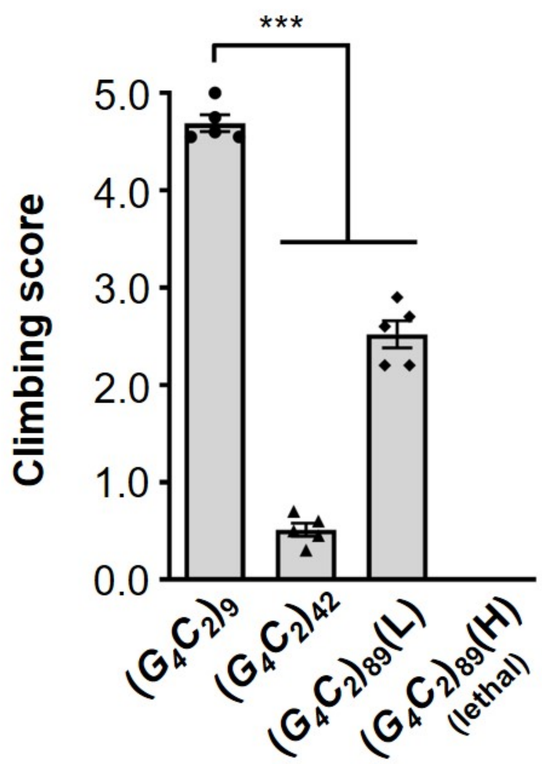
***
Climbing score
5.0
4.0
3.0
2.0
1.0
0.0
(G4C2)9
(G4C2)42
(G4C2)89(L)
(G4C2)89(H)
(lethal)

E

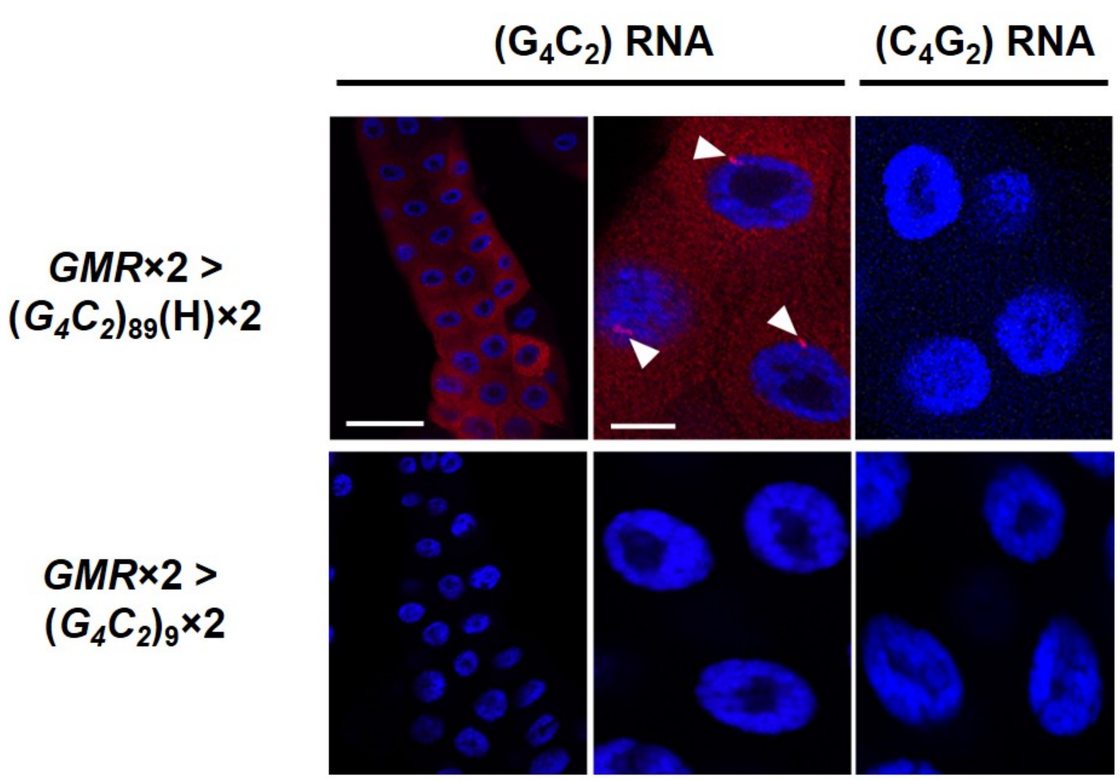
(G4C2) RNA
(C4G2) RNA
GMR×2 >
(G4C2)89(H)×2
GMR×2 >
(G4C2)9×2

F

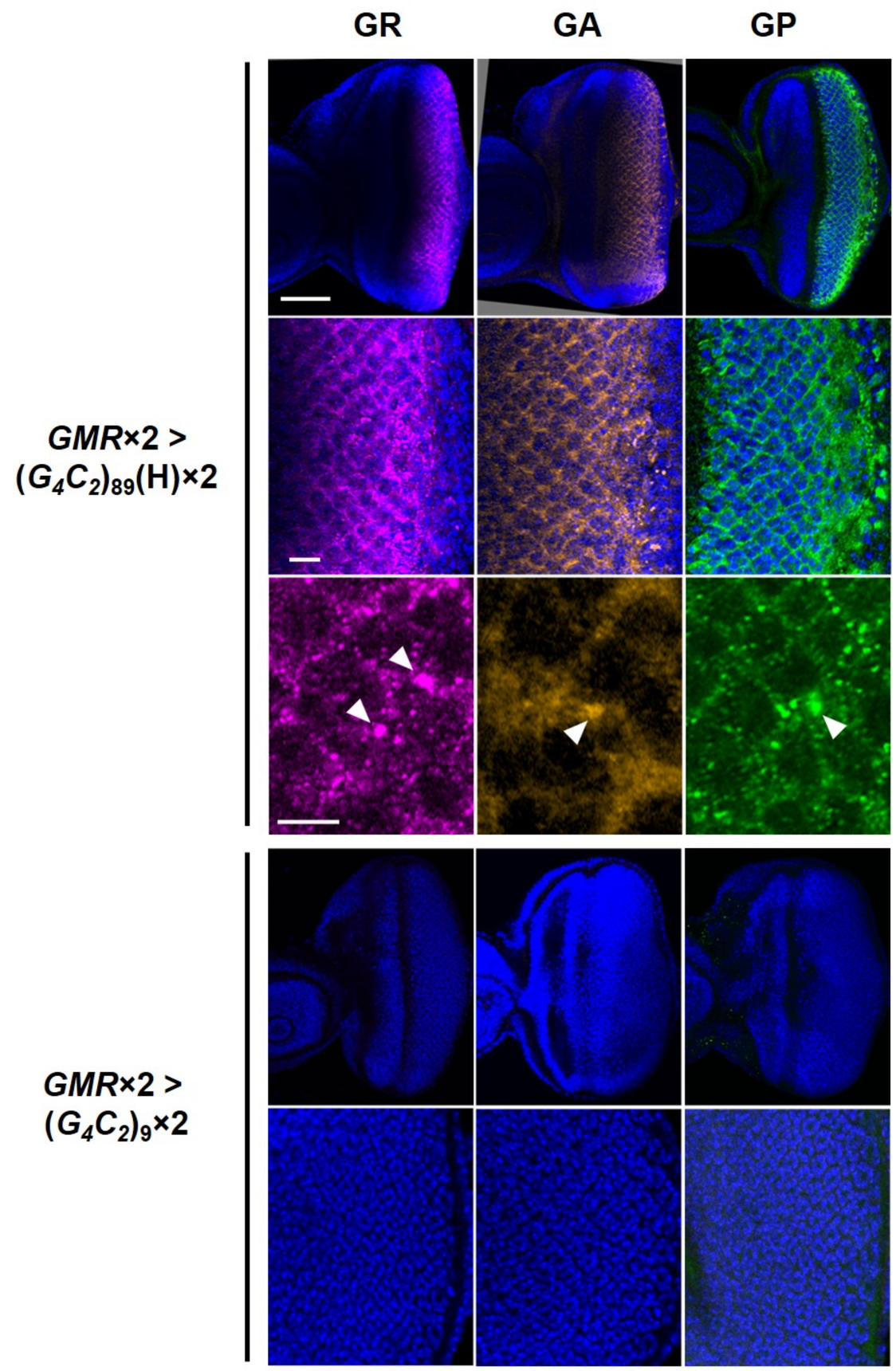
GR
GA
GP
GMR×2 >
(G4C2)89(H)×2
GMR×2 >
(G4C2)9×2

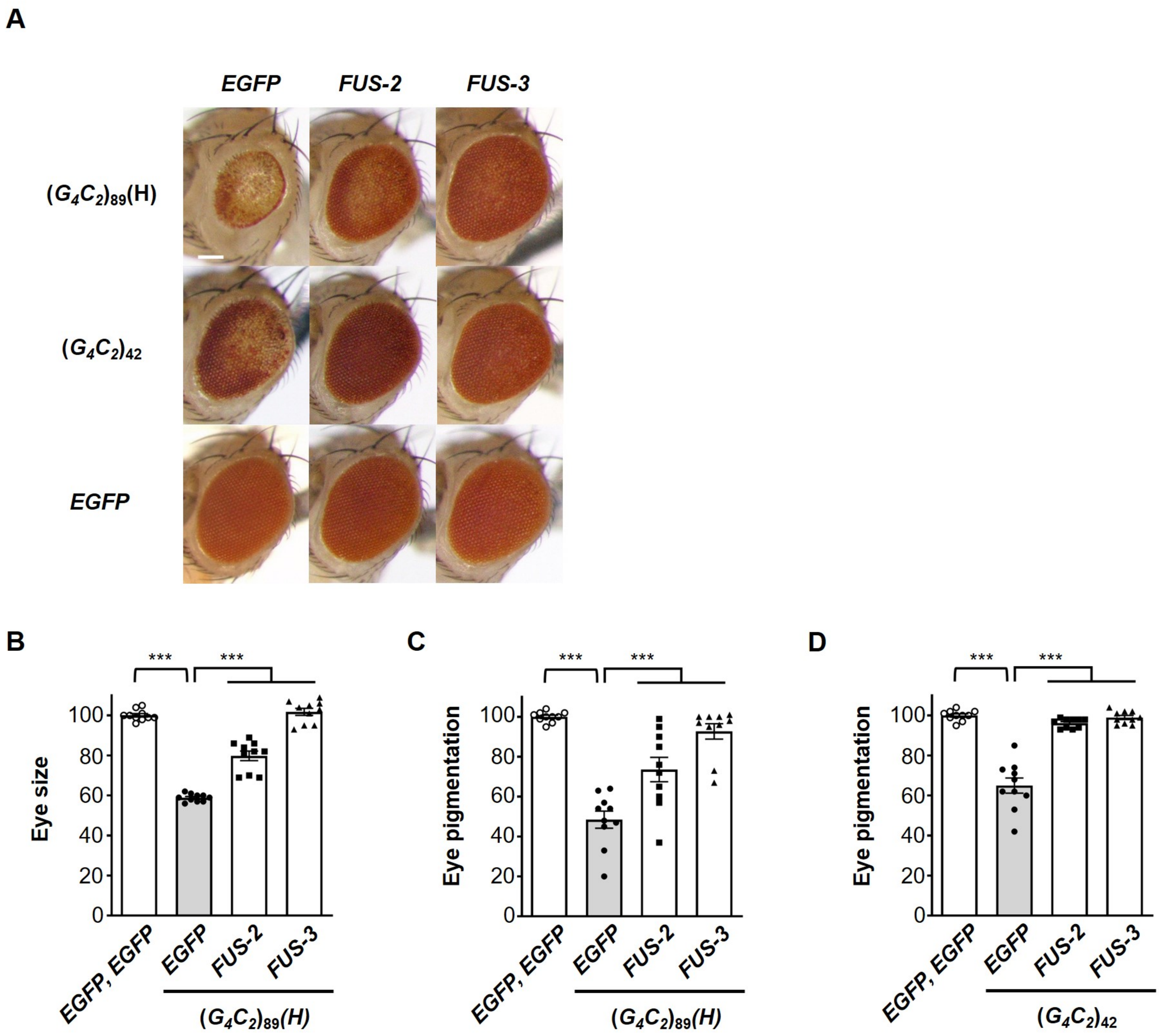
A
EGFP
FUS-2
FUS-3
(G4C2)89(H)
(G4C2)42
EGFP
B
Eye size
***
***
100
80
60
40
20
0
EGFP, EGFP
EGFP
FUS-2
FUS-3
(G4C2)89(H)
C
Eye pigmentation
***
***
100
80
60
40
20
0
EGFP, EGFP
EGFP
FUS-2
FUS-3
(G4C2)89(H)
D
Eye pigmentation
***
***
100
80
60
40
20
0
EGFP, EGFP
EGFP
FUS-2
FUS-3
(G4C2)42

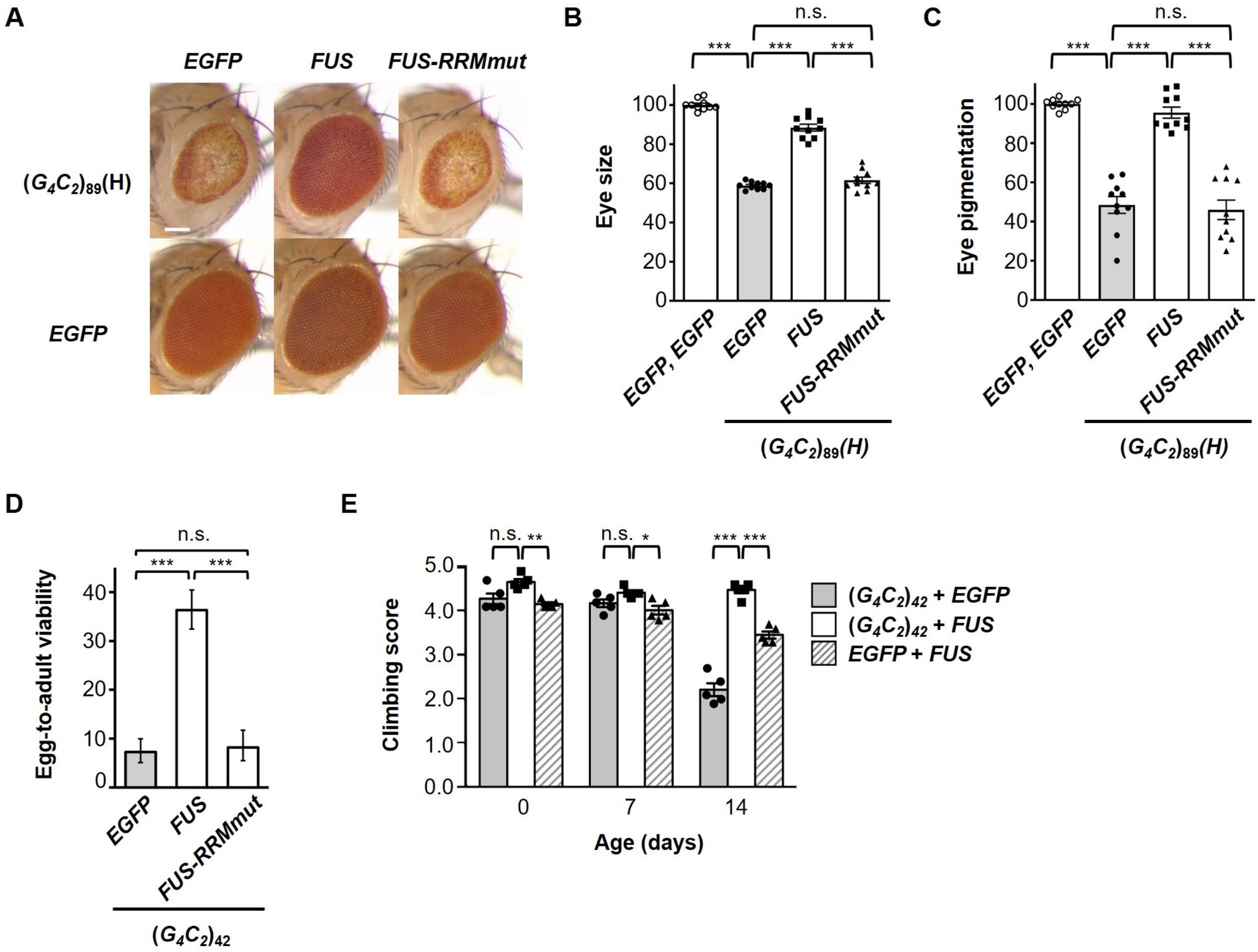
A
EGFP
FUS
FUS-RRMmut
(G4C2)89(H)
EGFP
B
n.s.
***
***
***
Eye size
100
80
60
40
20
0
EGFP, EGFP
EGFP
FUS
FUS-RRMmut
(G4C2)89(H)
C
n.s.
***
***
***
Eye pigmentation
100
80
60
40
20
0
EGFP, EGFP
EGFP
FUS
FUS-RRMmut
(G4C2)89(H)
D
n.s.
***
***
Egg-to-adult viability
40
30
20
10
0
EGFP
FUS
FUS-RRMmut
(G4C2)42
E
n.s. **
n.s. *
*** ***
Climbing score
5.0
4.0
3.0
2.0
1.0
0.0
0
7
14
Age (days)
(G4C2)42 + EGFP
(G4C2)42 + FUS
EGFP + FUS

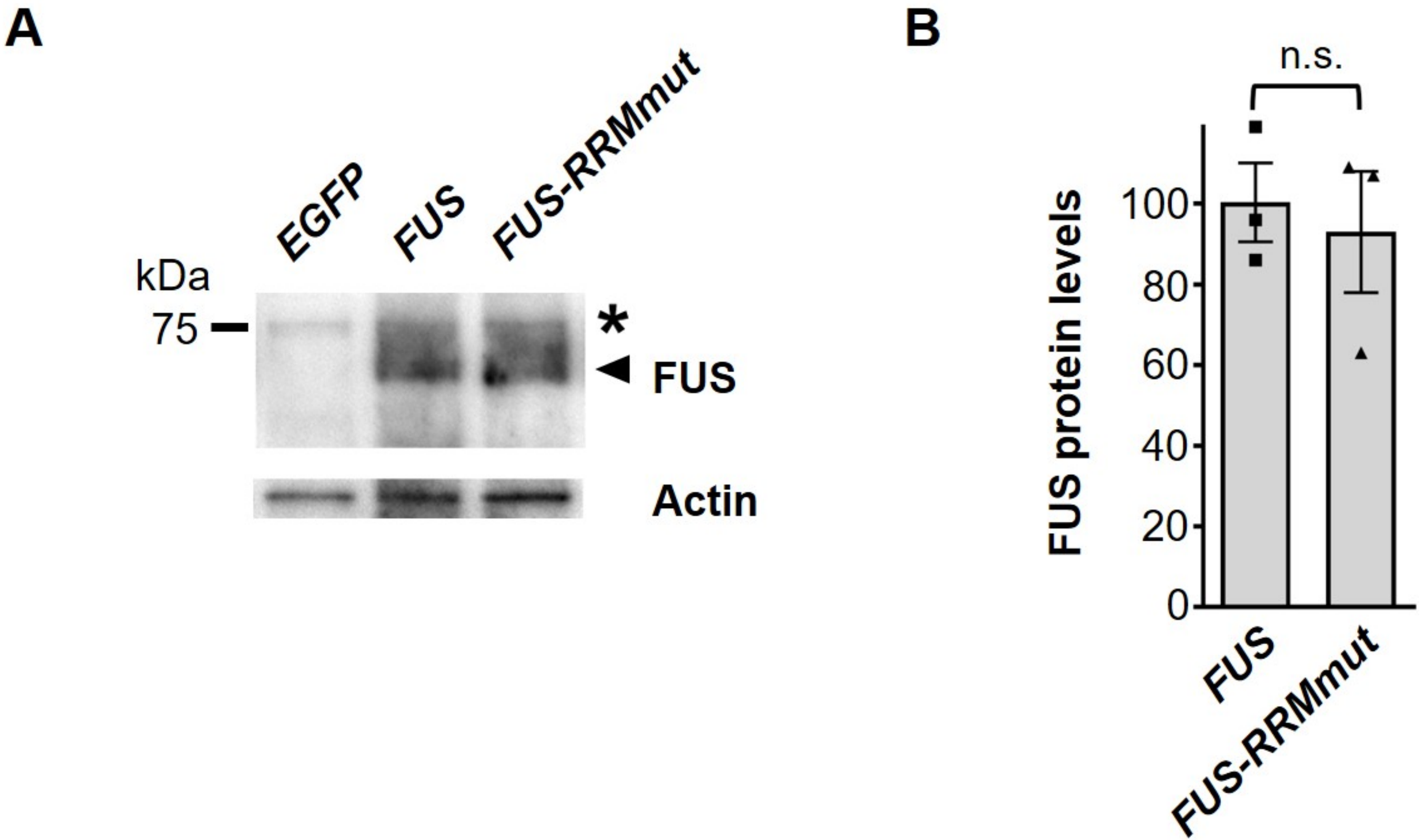
A
EGFP
FUS
FUS-RRMmut
kDa
75
*
FUS
Actin
B
n.s.
FUS protein levels
100
80
60
40
20
0
FUS
FUS-RRMmut

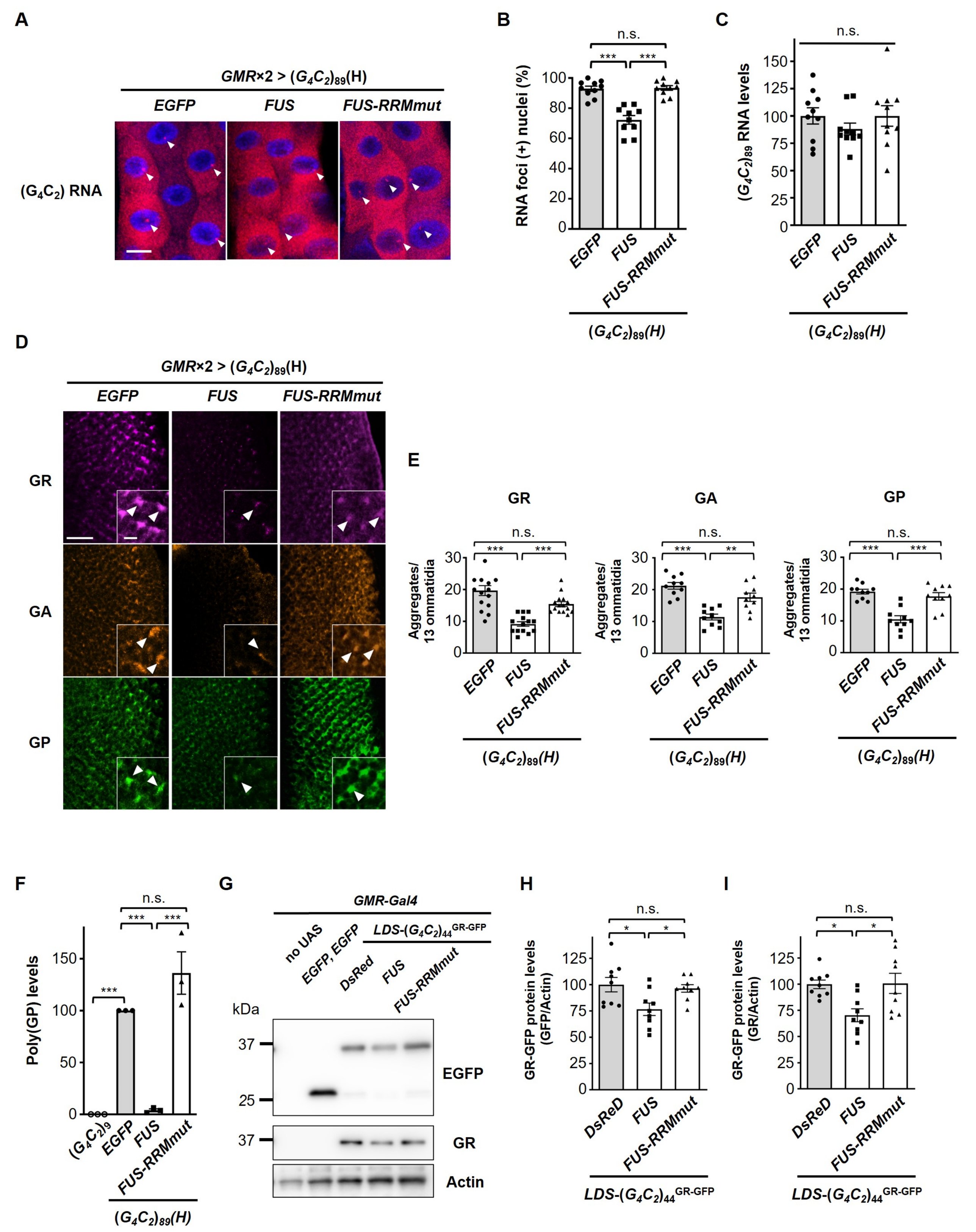
A
GMR×2 > (G4C2)89(H)
EGFP
FUS
FUS-RRMmut
(G4C2) RNA
B
n.s.
***
***
RNA foci (+) nuclei (%)
100
80
60
40
20
0
EGFP
FUS
FUS-RRMmut
(G4C2)89(H)
C
n.s.
(G4C2)89 RNA levels
150
125
100
75
50
25
0
EGFP
FUS
FUS-RRMmut
(G4C2)89(H)
D
GMR×2 > (G4C2)89(H)
EGFP
FUS
FUS-RRMmut
GR
GA
GP
E
GR
GA
GP
n.s.
***
**
Aggregates/
13 ommatidia
30
20
10
0
EGFP
FUS
FUS-RRMmut
(G4C2)89(H)
F
n.s.
***
***
Poly(GP) levels
150
100
50
0
(G4C2)9
EGFP
FUS
FUS-RRMmut
(G4C2)89(H)
G
GMR-Gal4
no UAS
EGFP, EGFP
LDS-(G4C2)44GR-GFP
DsRed
FUS
FUS-RRMmut
kDa
37
25
EGFP
37
GR
Actin
H
n.s.
*
GR-GFP protein levels
(GFP/Actin)
125
100
75
50
25
0
DsReD
FUS
FUS-RRMmut
LDS-(G4C2)44GR-GFP
I
n.s.
*
GR-GFP protein levels
(GR/Actin)
125
100
75
50
25
0
DsReD
FUS
FUS-RRMmut
LDS-(G4C2)44GR-GFP

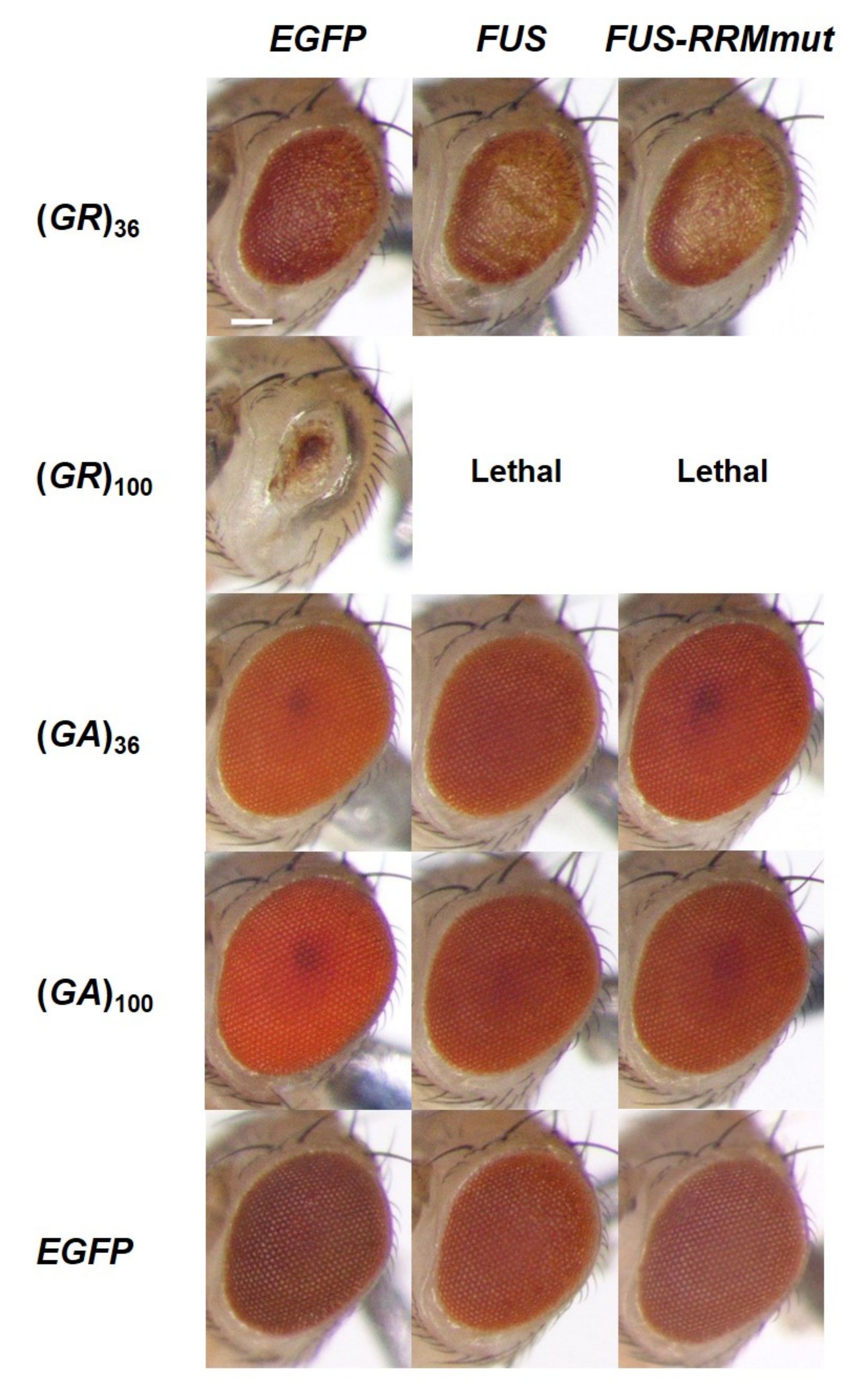
EGFP
FUS
FUS-RRMmut
(GR)36
(GR)100
Lethal
Lethal
(GA)36
(GA)100
EGFP

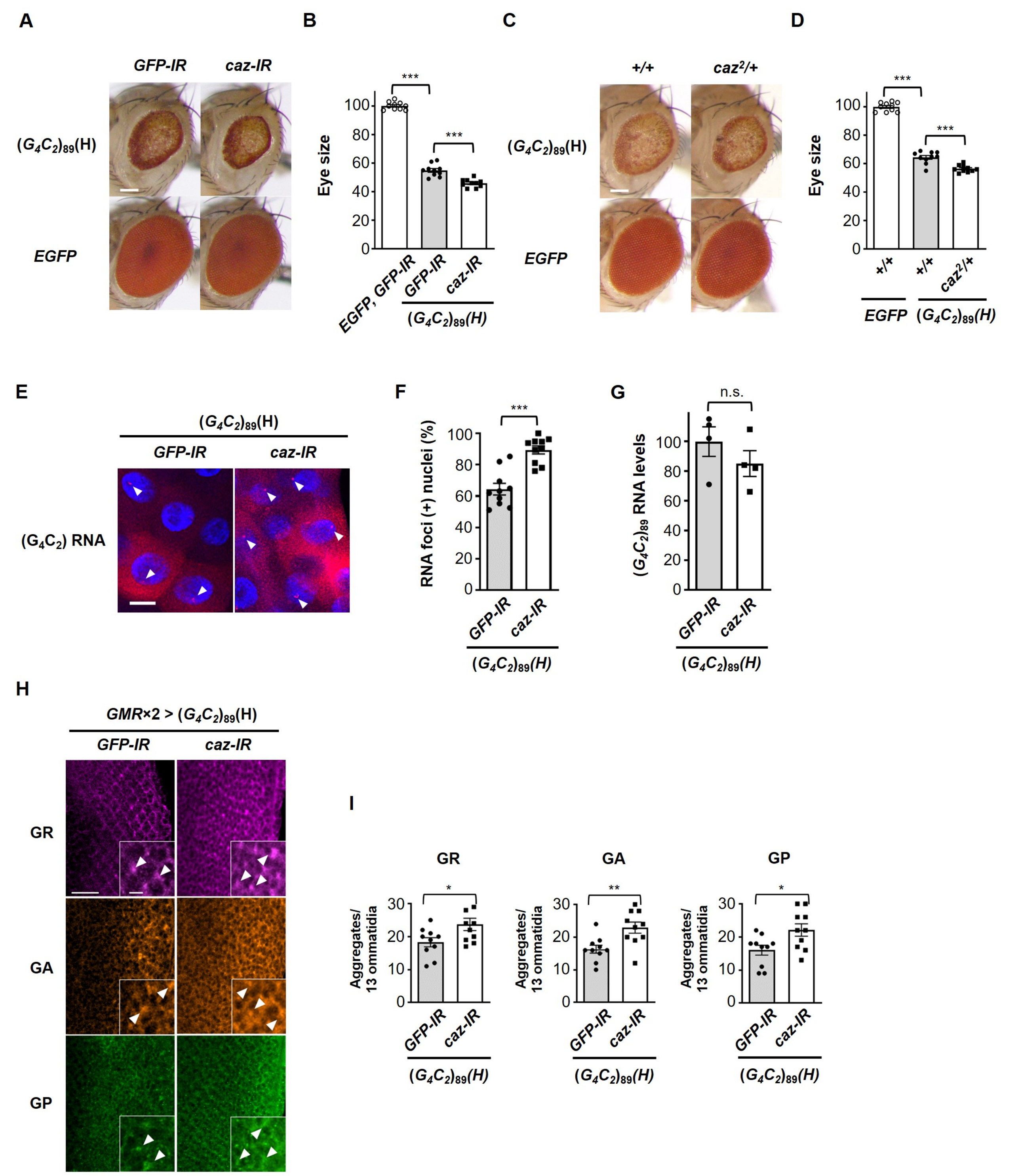
A
GFP-IR
caz-IR
(G4C2)89(H)
EGFP
B
Eye size
***
***
EGFP, GFP-IR
GFP-IR
caz-IR
(G4C2)89(H)
C
+/+
caz2/+
(G4C2)89(H)
EGFP
D
Eye size
***
***
+/+
+/+
caz2/+
EGFP
(G4C2)89(H)
E
(G4C2)89(H)
GFP-IR
caz-IR
(G4C2) RNA
F
RNA foci (+) nuclei (%)
***
GFP-IR
caz-IR
(G4C2)89(H)
G
n.s.
(G4C2)89 RNA levels
GFP-IR
caz-IR
(G4C2)89(H)
H
GMR×2 > (G4C2)89(H)
GFP-IR
caz-IR
GR
GA
GP
I
GR
GA
GP
Aggregates/ 13 ommatidia
*
**
*
GFP-IR
caz-IR
(G4C2)89(H)

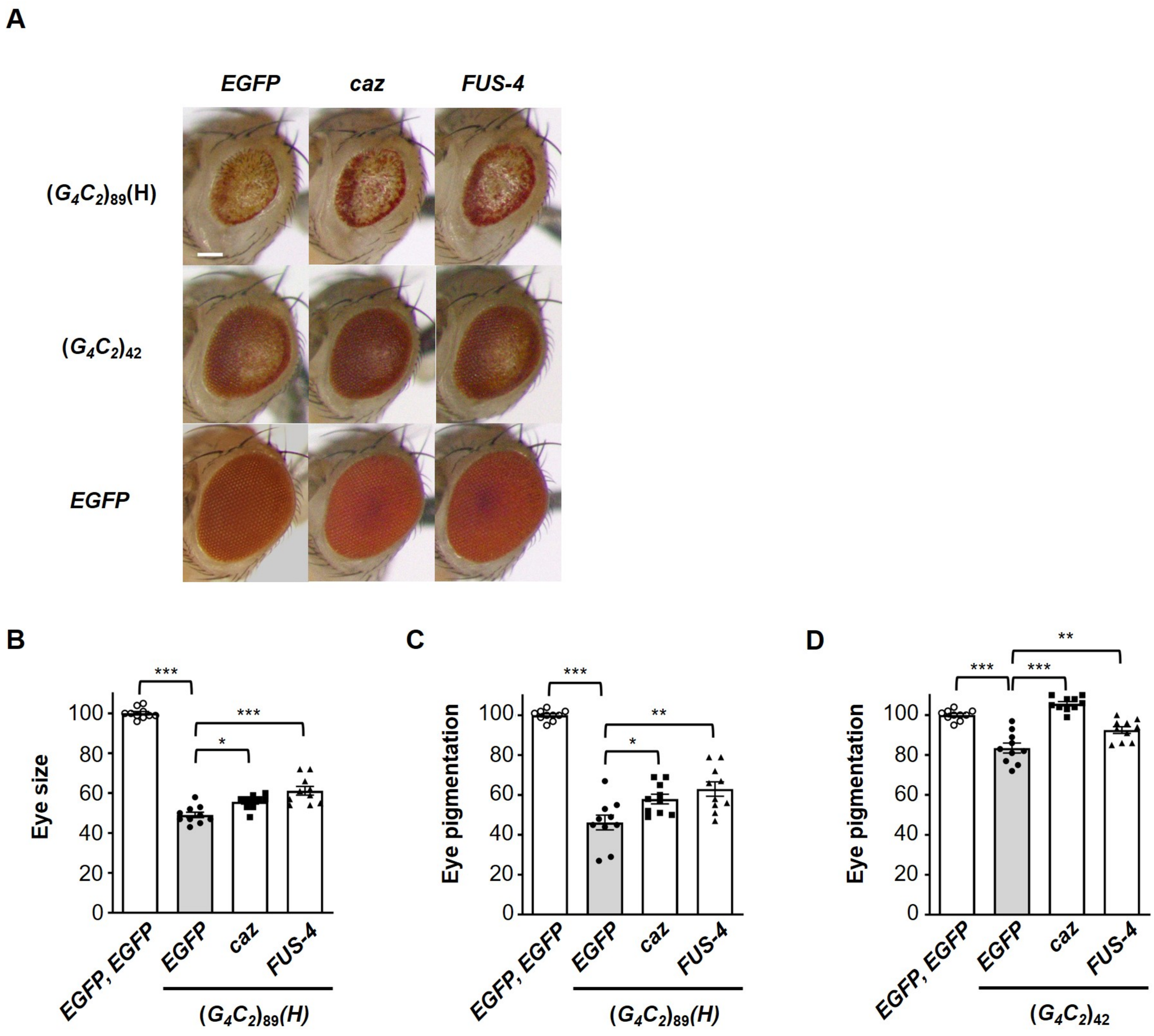
A
EGFP
caz
FUS-4
(G4C2)89(H)
(G4C2)42
EGFP
B
Eye size
***
***
*
EGFP, EGFP
EGFP
caz
FUS-4
(G4C2)89(H)
C
Eye pigmentation
***
**
*
EGFP, EGFP
EGFP
caz
FUS-4
(G4C2)89(H)
D
Eye pigmentation
**
***
***
EGFP, EGFP
EGFP
caz
FUS-4
(G4C2)42

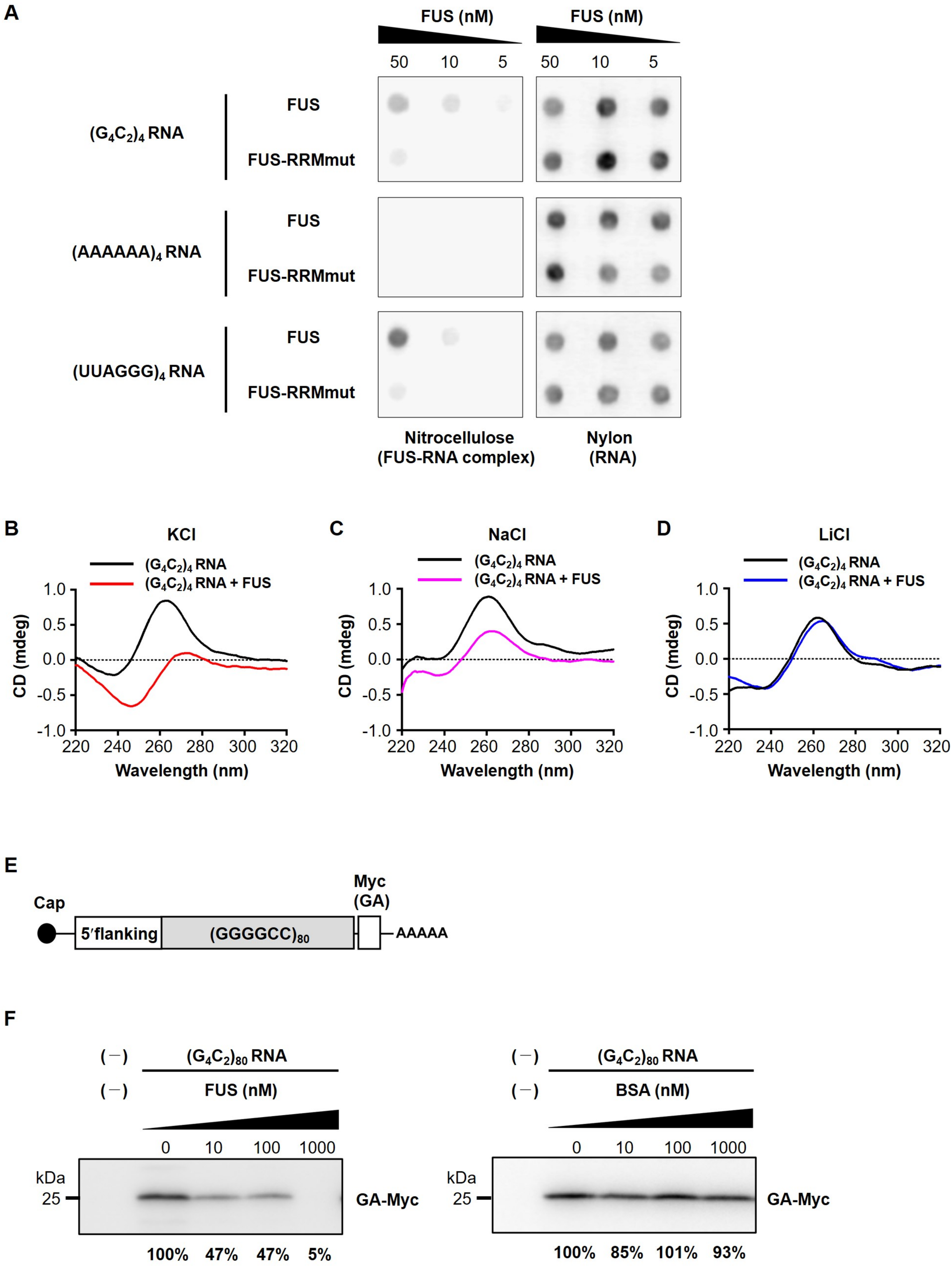
A
FUS (nM)
50 10 5
FUS (nM)
50 10 5
(G4C2)4 RNA
FUS
FUS-RRMmut
(AAAAAA)4 RNA
FUS
FUS-RRMmut
(UUAGGG)4 RNA
FUS
FUS-RRMmut
Nitrocellulose
(FUS-RNA complex)
Nylon
(RNA)
B
KCl
(G4C2)4 RNA
(G4C2)4 RNA + FUS
CD (mdeg)
Wavelength (nm)
C
NaCl
(G4C2)4 RNA
(G4C2)4 RNA + FUS
CD (mdeg)
Wavelength (nm)
D
LiCl
(G4C2)4 RNA
(G4C2)4 RNA + FUS
CD (mdeg)
Wavelength (nm)
E
Cap
5′flanking
(GGGGCC)80
Myc
(GA)
AAAAA
F
(−) (G4C2)80 RNA
(−) FUS (nM)
0 10 100 1000
kDa
25
GA-Myc
100% 47% 47% 5%
(−) (G4C2)80 RNA
(−) BSA (nM)
0 10 100 1000
kDa
25
GA-Myc
100% 85% 101% 93%

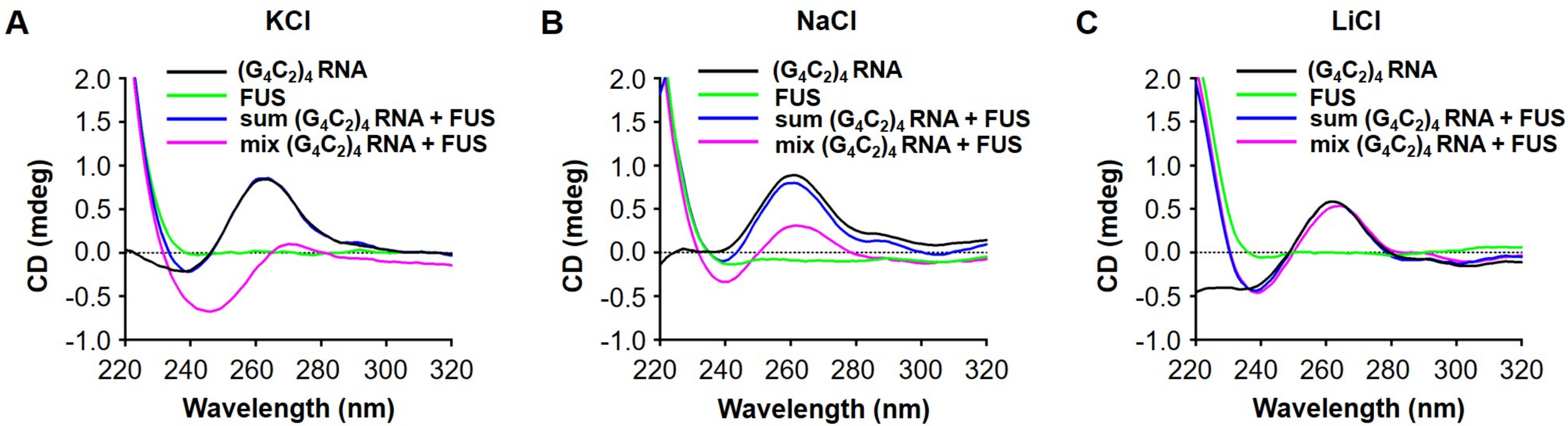
A
KCl
B
NaCl
C
LiCl
$(G_4C_2)_4$ RNA
FUS
sum $(G_4C_2)_4$ RNA + FUS
mix $(G_4C_2)_4$ RNA + FUS
CD (mdeg)
2.0
1.5
1.0
0.5
0.0
-0.5
-1.0
220
240
260
280
300
320
Wavelength (nm)

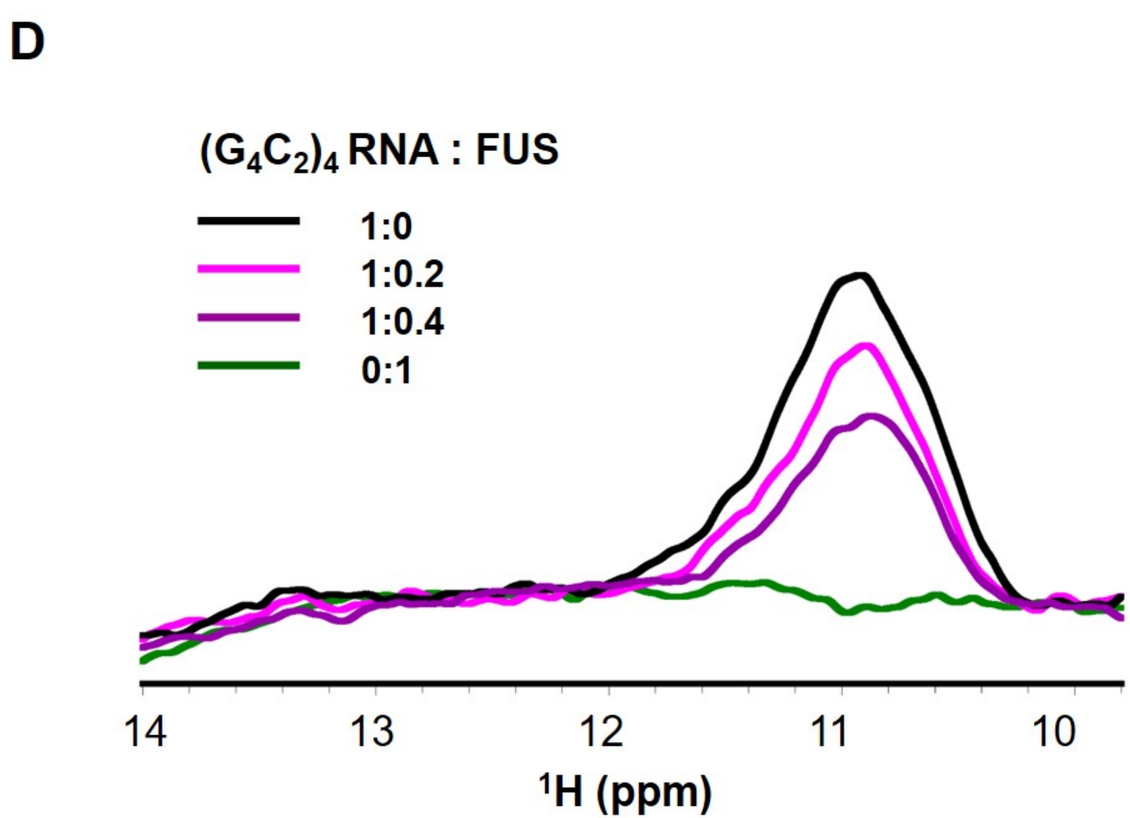
D
$(G_4C_2)_4$ RNA : FUS
1:0
1:0.2
1:0.4
0:1
14
13
12
11
10
^{1}H (ppm)

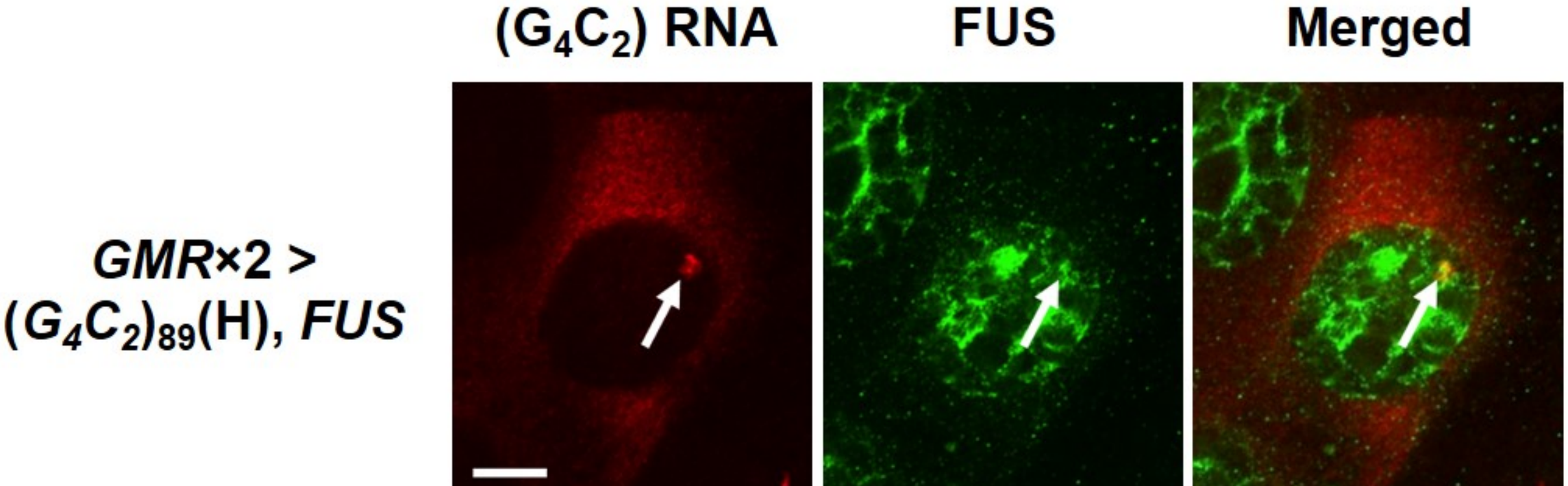
(G4C2) RNA
FUS
Merged
GMR×2 >
(G4C2)89(H), FUS

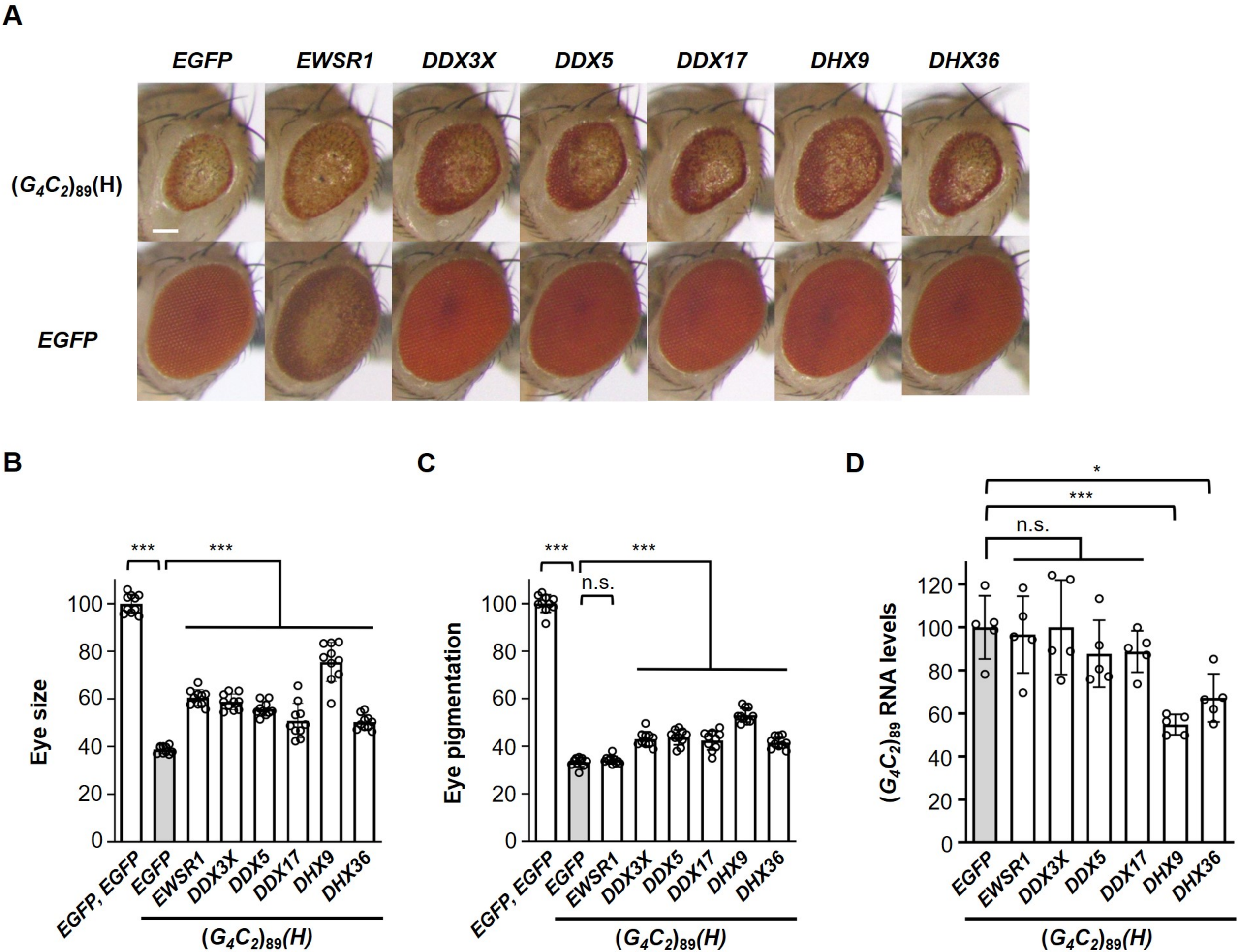
A
EGFP
EWSR1
DDX3X
DDX5
DDX17
DHX9
DHX36
(G4C2)89(H)
EGFP
B
Eye size
***
***
EGFP, EGFP
EGFP
EWSR1
DDX3X
DDX5
DDX17
DHX9
DHX36
(G4C2)89(H)
C
Eye pigmentation
***
n.s.
***
EGFP, EGFP
EGFP
EWSR1
DDX3X
DDX5
DDX17
DHX9
DHX36
(G4C2)89(H)
D
(G4C2)89 RNA levels
*
***
n.s.
EGFP
EWSR1
DDX3X
DDX5
DDX17
DHX9
DHX36
(G4C2)89(H)